Chemical weathering signatures from Mt. Achernar Moraine, Central Transantarctic Mountains I: Subglacial sediments compared with underlying rock

Joseph A Graly[1,2], Kathy J Licht[2], Nicole A Bader[2], David L Bish[3]

1: Northumbria University, Geography and Environmental Sciences, Newcastle Upon Tyne, UK
2: Indiana University Purdue University Indianapolis, Earth Sciences, Indianapolis, IN, USA
3: Indiana University, Earth and Atmospheric Sciences, Bloomington, IN, USA

Abstract

In order to determine chemical weathering rates on the subglacial land surface of Antarctica, we compare the composition and mineralogy of freshly emerging fine sediments to that of the underlying bedrock, as represented by glacially derived cobble-sized clasts. Samples were collected from Mt. Achernar Moraine, a large blue ice moraine, where subglacial material naturally emerges through sublimation of the surrounding ice. Both rocks and sediments were analyzed for total elemental composition, mineral abundance by X-ray diffraction, and by sequential extractions targeting chemical weathering products. The fine sediment fraction is significantly enriched in chemical weathering products and depleted in primary minerals compared with the cobble clasts. The alteration pathways consist primarily of the development of smectite, kaolinite, carbonate minerals, and amorphous material. Extensive Fe oxidation is evidenced by a decline in magnetic susceptibility and by increases in extractable Fe. If we assume the only input into the subglacial system is the water and ice-trapped gas supplied by basal melt, the net chemical alteration is explained through oxidation of organic matter equal to ~0.7% of the bedrock mass and subsequent carbonation weathering. The underlying sedimentary rock is sufficiently rich in organic matter for this pathway to be plausible. For the O_2 that is oxidizing organic matter to be supplied by basal meltwater, water fluxes would need to be three orders of magnitude larger than sediment fluxes. Independent models of basal melt and sediment transport at our field site confirm that such a difference between water and sediment flux is likely at the study site. The rate of subglacial carbonation weathering inferred from the Mt. Achernar Moraine site may be

comparable to that found in high latitude subaerial environments. If Mt. Achernar Moraine is typical of other Antarctic sites, the subglacial land surface of Antarctica does play a role in global geochemical cycling.

Introduction

Chemical weathering is a process fundamental to the cycling of earth materials from the atmosphere to the land surface and from the land surface to the oceans. Contemporary fluxes from chemical weathering have been widely assessed from river chemistry (Gaillardet et al., 1999), and fluxes over geological time scales have been assessed through a variety of isotope systems (Kump et al., 2000). The glacial component of chemical weathering has been mostly assessed in alpine regions, where outlet streams integrate subglacial chemistry (Anderson et al., 1997; Hodson et al., 2000). Glacial discharge waters were once thought to play a relatively minor role in global geochemical cycling due to the predominance of highly reactive trace components in their chemistry (Tranter, 2003). However, work on Greenland and other large glaciohydraulic systems has shown substantially greater silicate weathering fluxes compared with alpine systems (Graly et al., 2014; Hawkings et al., 2017; Wadham et al., 2010), and new analyses have revised the geochemical impact of alpine systems upward (Graly et al., 2017; Torres et al., 2017). Because terrestrial proglacial fluvial discharge from Antarctic ice is extremely limited, Antarctic subglacial weathering has been excluded from chemical mass balance estimates that focus on riverine fluxes (i.e. Gaillardet et al., 1999).

Subglacial chemical fluxes within and from Antarctica's landscape have only been measured at a few locations (i.e. Michaud et al., 2016; Skidmore et al., 2010). As the subglacial environment of Antarctica accounts for ~10% of Earth's land surface, continent-wide assessment of its chemical fluxes is important to a global understanding of geochemical cycles. Most of the continent has liquid water at the glacier bed sourced from basal melt (Pattyn, 2010). This glacial meltwater contains atmospheric gases

53 trapped during initial ice formation, with O_2 capable of oxidizing organic matter and sulfides to form the
54 acids driving chemical weathering (Graly et al., 2017). For the carbon cycle, this pathway potentially
55 delivers a significant load from fossil carbon to the ocean atmosphere system (Petsch, 2014; Wadham et
56 al., 2012). However, concentrations of dissolved solutes, which track chemical fluxes, are difficult to
57 measure in Antarctica's subglacial environment. Inference to continent-wide rates of chemical alteration
58 must presently rely on drilling access to subglacial water (e.g. Michaud et al., 2016) or on the rare and
59 perhaps atypical cases where such water naturally emerges (e.g. Badgeley et al., 2017).

60 The alternative approach, explored here, is to analyze subglacial sediment rather than subglacial
61 water. Glacial sediments originate from the comminution of rock underneath ice and once formed, such
62 sediments can be chemically altered in the subglacial environment by subglacial meltwater and the
63 atmospheric gases trapped therein (Crompton et al., 2015). The degree of chemical alteration is
64 reflected by the mineralogical differences between rock and sediment. Where it is possible to compare
65 subglacial sediment to underlying rock, the mass of the minerals newly formed within subglacial
66 sediment is measured and compared to the mass loss of primary minerals. The total chemical
67 weathering flux is inferred from this mineral mass balance. We consider minerals that are typically
68 found in soil such as clays, oxyhydroxides, carbonates, and amorphous material to be like candidates for
69 neoformation within the subglacial environment. These minerals form in a wide range of soil settings
70 the world over, however they may also be inherited from underlying rock (Wilson, 1999). Neoformation
71 or authigenesis is inferred where the mineral is significantly more abundant in subglacial sediment than
72 in the underlying rock. It is further indicated where we see changes in mineral composition or layer
73 stacking order within the crystal lattice between rock and sediment (Reynolds, 1989). These changes in
74 sediment composition are translated into weathering rates where the rate of sediment delivery from
75 the ice sheet can be observed or modeled.

We present a case study of a mineralogical method to assess subglacial chemical weathering fluxes at a site in the central Transantarctic Mountains where subglacial sediments emerge at the surface of a blue ice moraine. Blue ice moraines are formed where sublimation-driven ablation causes sediment from within the glacier to accumulate on the surface of the ice (Bintanja, 1999). Our study site, Mt Achernar Moraine (84.2° S, 161° E), is located near the head of Law Glacier, where the ice first crosses the Transantarctic Mountains. Studies here have characterized till composition and provenance (Bader et al., 2017), soil formation (Scarrow et al., 2014), and the timing of till accumulation (Graly et al., 2018b; Kaplan et al., 2017). Ground penetrating radar measurements at the site have shown that the sediment in the moraine sources from the glacier bed and accumulates laterally over time (Kassab et al., 2020). Stable isotopes of O and H in the moraine's ice suggest that sediment entrainment occurred in the presence of liquid subglacial water, upstream from the moraine, at the margin of the polar plateau (Graly et al., 2018c).

The exposed rocks of the central Transantarctic Mountains have been characterized at many locations (Faure and Mensing, 2010), however the bedrock geology under the ice is not directly known. The exposed rocks at Mt. Achernar belong to the spatially extensive Beacon Supergroup – a terrestrially deposited, alluvial sequence of sandstone, siltstone, and shale (Barrett et al., 1986). The lower formations of the Beacon Supergroup in this region derive from rocks associated with the Gondwana margin; sedimentary sources then shifted to a West Antarctic arc-derived volcanoclastic sediment source and finally to a mix of East and West Antarctic sources (Elliot et al., 2017). The Beacon is pervasively intruded by mafic sills of the Ferrar Dolerite, with local contact metamorphism to low temperature (200-300˚ C) hornfels facies. Burial diagenesis alongside fluids from the contact metamorphic event have caused widespread formation of illite, chlorite, and, in some cases, zeolite cements (Bernet and Gaupp, 2005). Locally, Mt. Achernar consists of Ferrar Dolerite interlayered with the lower Buckley Formation of the Beacon Supergroup (Isbell, 1990). Sedimentary rock clasts within the

moraine are dominantly from the lower formations of the Beacon Supergroup (i.e. Mackellar, Fairchild, and L. Buckley), the Ferrar Dolerite, and few erratics (Bader et al., 2017). Detrital zircon analyses confirm that only lower Beacon (i.e. East Antarctic source) material is supplied to the site (Bader et al., 2017).

At Mt. Achernar Moraine, fine sediment emerges together with rock clasts of a range of sizes, including pebbles, cobbles, and boulders. By analyzing both cobble size clasts, presumed to represent plucked bedrock from the catchment, and fine sediment (<63 μm), we assess the chemical alteration that occurs in the subglacial environment. Due to surface area effects, large rock clasts are minimally altered by the chemical processes of the subglacial environment compared with fine sediments such as silt and clay-sized particles (Graly et al., 2016). Chemical alteration is not visible in hand samples of freshly emerging cobble-sized clasts (Bader et al., 2017). The site has minimal potential for inherited preglacial or interglacial weathering within the emerging subglacial sediments. It is proximal to the polar plateau (El. ~1800 m), with little exposed rock upstream. The regional subglacial environment is high elevation (Jamieson et al., 2010) and Pliocene interglacial exposure in this area is not suggested by numerical models (Pollard and DeConto, 2009; Scherer et al., 2016). Similar sites occur at numerous locations around Antarctica where blue ice moraines form at the base of nunataks (Bintanja, 1999). This suggests that methods developed in this study could provide insights into subglacial weathering processes and fluxes for many regions around the continent.

Methods

During 2010 and 2015 field seasons, samples were collected from Mt. Achernar Moraine ranging from water-saturated sediment freshly emerging from melting ice to dry till with more than 500 ka of surface exposure. However, we limited our analysis here to ten samples where active ablation processes were ongoing and moisture from the ablating ice remained (Figure 1). Sediment samples were collected by shoveling sediment with an inert plastic scoop into plastic bags. Moisture was removed by freeze

drying. A grain size analysis was performed on the <1 mm fraction using a Malvern Mastersizer 2000 (Table S1). At five sites, an adjoining pebble and cobble sample (~30-70 mm diameter clasts) was collected from a square meter surface area. The pebble count data and some of the grain size data were previously reported in Bader et al. (2017).

Twelve cobble samples representative of rock types common on the moraine surface were selected from the pebble and cobble samples. Igneous clasts that represent the ubiquitous Ferrar Dolerite sills represent 60% of the pebble and cobble clasts within the freshly emerging (<10 ka surface exposure) section of the moraine (Bader et al., 2017). The samples appeared relatively homogenous by visual inspection, and three dolerites were selected for detailed analyses. One dolerite (Rock 1) was striated and faceted and therefore had clear influence of transport in the subglacial environment. The other two samples contrast coarse-grained (Rock 2) and fine-grained (Rock 3) dolerite. We analyzed two sandstones (Rocks 4-5), two siltstones (Rocks 6-7), one striated and polished black argillite (Rock 8), one black argillite without signs of subglacial physical alteration (Rock 9), two shales (Rocks 10-11), and one white argillite (Rock 12). These samples were crushed and ground to <100 µm grain size. The average of these 12 compositions was weighted to determine the total composition of the underlying rock.

We performed a series of analyses on the crushed rocks and glacial sediments in order to determine the abundance of chemical weathering products. Unless otherwise stated, results are reported from the whole crushed sample of the rocks and the <63 µm fraction of the sediment, which was isolated from the bulk sample by dry sieving to preserve any water-soluble material in the sample. Major and trace elemental composition was analyzed by total dissolution of a fused sample, and inductively coupled plasma mass spectrometry by Actlabs. Eighteen standards, each appropriate to various ranges of elements, were included in the mass spectrometry analysis (Tables S2, S3). Magnetic susceptibility was analyzed on the crushed rock and on the 63-250 µm fraction of the sediment, employing a Barrington MS2 meter. Values were converted to wt. % magnetite based on comparison

148 with a 1% magnetite standard. The abundance and speciation of salts and sulfates, carbonates,
149 amorphous oxyhydroxides, and crystalline oxides were analyzed by a sequence of progressively stronger
150 chemical extractions of the water-soluble, acetic acid-soluble, hydrochloric acid-soluble, and
151 hydroxylamine hydrochloride-soluble fractions respectively on one-g aliquots of each sample (e.g.
152 Wiederhold et al., 2007). The extraction sequence consisted of: 1) milli-Q water (H_2O) for 2 hours; 2)
153 0.11 M acetic acid (CH_3COOH) for 16 hours; 3) 0.5 M hydrochloric acid (HCl) for 24 hours; 4) 1 M
154 hydroxylamine hydrochloride (NH_2OH-HCl) in 1 M HCl for 4 hours. For each step in the sequence, the 1-g
155 sediment aliquot was mixed with 40 ml of extractant and agitated for a set time length. For the H_2O,
156 CH_3COOH, and HCl extractions, samples were placed on a vibrating table at room temperature, set at a
157 speed sufficient to keep material in suspension. During the NH_2OH-HCl extraction, the samples were
158 placed in a 70˚ C ultrasonic bath. The samples were removed every 10 minutes and manually agitated
159 until all the material returned to suspension and were then returned to the bath. After each extraction
160 step, the samples were centrifuged for 15 minutes at 3300 RPM. The supernatant was then decanted
161 and stored for analysis. The sediment was mixed with 20 ml of milli-Q water and agitated for 20
162 minutes. The sample was again centrifuged and the rinse water decanted and discarded. All extracts
163 were measured in triplicate for major elements on a Perkin-Elmer Optima 7000 inductively coupled
164 plasma – optical emission spectrometer (ICP-OES).

165 Mineral abundance was independently measured through powder X-ray diffraction and Rietveld
166 refinement. Samples were mixed with a 20 wt. % corundum standard (1 μm) and pulverized in an agate
167 mill. X-ray diffraction was performed on a Bruker D8 Discover instrument (Cu Kα), measuring from 2-70˚
168 2θ. The patterns were analyzed by Rietveld refinement (Bish and Post, 1989; Rietveld, 1969) with Topas
169 (Bruker AXS, version 5) software to quantitatively determine mineral abundances, with uncertainties
170 determined by the variance of the least squared fit. To further assess clay mineralogy, the <1 μm
171 fraction was isolated by settling out larger material in water. The suspended sediment portion was

concentrated by centrifuging and dried onto a zero-background slide. These clay isolates were analyzed in the 2-30˚ 2θ range. Each slide was subsequently placed in an ethylene glycol chamber for 48 hours and was analyzed again to assess the prevalence of expandable clays.

X-ray diffraction cannot detect or characterize amorphous material and material with high layer stacking disorder. However, a Rietveld refinement method performed with a corundum standard quantifies the abundance of this unmodeled component of a sample, which represents the amorphous component along with trace phases that are below detection by X-ray diffraction (Bish and Post, 1989). We assess the composition of this unmodeled component from the residual of the bulk composition from total dissolution less the mineral composition and abundances from the Rietveld refinement. The sequential extractions are also designed to primarily target these phases. As a test of both the X-ray diffraction and sequential extraction methods, we compared the total extracted content of each major element to the residual of the bulk elemental composition less the mineral composition and abundances determined by X-ray diffraction and Rietveld refinement.

Average rock and sediment compositions

For the analytical approaches employed, we assessed the magnitude and statistical significance of differences between the cobble-sized clasts and freshly emerging fine sediments. Because the cobble-sized clasts were chosen to represent the range of observed rock types, not their abundance, the arithmetic mean of the samples is not indicative of the actual average rock composition on the moraine. Thus, in order to more accurately explore the transformation between rock and fine sediment via geochemical modeling, we calculated an 'average' rock composition of the moraine using two different methods. For the 'pebble count' method, the composition of the cobble samples was weighted to their abundance among pebble and cobble sized clasts per square meter as described in Bader et al. (2017). The alternative is a 'mass balance' approach calculated by weighting the rock type abundances so that

196 generally immobile elements or minerals are conserved between the average rock composition and the
197 average composition of the <63 µm fraction. Unless otherwise noted, we treated difference between
198 populations as statistically significant when they passed a two tailed t test with p<=0.05.

199 Both methods of assessing average rock composition have advantages and limitations. Pebble
200 counts were performed to a high degree of precision (n>1500) (Bader et al. 2017). However, these
201 abundances may not be representative of underlying rock contribution as a whole as sedimentary rocks
202 with moderately weak cement are substantially less likely to be preserved in the pebble sized fraction
203 than igneous dolerites (Lee and Rutter, 2004). The mass balance method also could be potentially
204 unrepresentative, as certain elements will be selectively leached by subglacial chemical processes, and
205 physical processes may selectively comminute certain elements into the fine sediment fraction (Graly et
206 al., 2016).

207

208 *Geochemical mass balance*

209 This study is focusing on the two end member products of the physical and chemical processes
210 occurring beneath the ice: the cobble clasts that only have a thin surface subject to physical and
211 chemical alteration, and the <63 µm fraction which mixes detrital minerals that have been finely
212 comminuted by physical processes with authigenic clays and other newly formed minerals. From these
213 two end members we model the composition of the subglacial sediment and estimate the total loss and
214 gain in the abundance of each mineral species. We treat the sample as a closed system, into which only
215 water and air from ice melt can enter and only solutes can leave. Thus, any gain in a mineral's
216 abundance is balanced with the loss of minerals from which its elemental components derive. Where
217 loss on ignition is greater the <63 µm fraction than the rock, we model derivation from meltwater via
218 hydration and oxidation reactions. Where chemical elements are more abundant in the rock than the
219 <63 µm fraction, we model loss to solutes.

The mass balance methods described in this paper are new, but developed within the context of mineral mass balance approaches that have been previously employed in a variety of settings (e.g. Chadwick et al., 1990; Moulton et al., 2000). In order to model the total chemical alteration for the entire sediment sample, we need to make assumptions about the composition of the sand, granule and pebble fractions, whose compositions are not analyzed in this study. To do so, we assume that the polymineralic fragments within the sand-pebble size fractions have the same composition as the cobble clasts and that the single-mineral portion of the sand fraction has the same composition as the silt. Clay minerals are assumed to be absent from the silt sized fraction, as the breakdown of minerals along grain boundaries is assumed to be complete at silt size, leaving any detrital clays in the clay-sized fraction (Haldorsen, 1981). These assumptions leave any chemical alteration that occurs within intermediate-sized, multi-mineral grains unassessed in our analysis.

Mineral mass balance calculations between the cobble clasts and the disaggregated, monomineralic fraction were performed by reweighting the abundance of each of the mineral species analyzed in the <63 µm fraction through the following:

$$M_{Calc} = \left[W_{clay} + \frac{m_{2-63}+m_{>63*}}{m_{2-63}}(1 - W_{clay})\right]\frac{m_{<63}}{m_{<2}+m_{2-63}+m_{>63*}}M_{meas} \quad (1)$$

where M_{Calc} is the calculated mass of a mineral in the subglacial sediment as a whole, M_{Meas} is the mass of that mineral measured within the <63 µm fraction, $m_{<2}$ is the percent weight of the bulk sample that is <2 µm (i.e. clay sized), m_{2-63} is the percent weight of the sample that is between 2 and 63 µm (i.e. silt sized), $m_{>63*}$ is the percent weight of the sample that is >63 µm but not composed of lithic fragments, and W_{clay} is the fraction of the measured mineral species that falls within the <2 µm fraction. $m_{<2}$ and m_{2-63} are determined from the particle size data. $m_{>63*}$can either be determined by grain counting or by mass balance assuming conservation of a particular mineral or minerals. We used mass balance, assuming illite conservation (i.e. that illite is not subglacially formed or chemically weathered within the system) and verified the mass balance result by light microscope examination of

244 the sand sized fraction to determine the abundance of polymineralic in 5 samples. Particles greater than
245 sand sized were assumed to be entirely lithic fragments. For clay minerals, we assumed a W_{clay} of 1. For
246 quartz and zeolites, we estimate W_{clay} based on the quartz and zeolite abundance observed in the clay
247 mount samples, as opposed to bulk powder diffraction samples. For products observed through the
248 sequential extractions, we calculated a single W_{clay} that allows the clay mass observed from particle
249 size analysis to equal the clay mass inferred from mineralogy. For all other minerals, we assumed W_{clay}
250 to be 0.

251 To compare the loss in rock-forming minerals with the gain in clays, we calculated the
252 stoichiometric chemical weathering reactions that would govern the transformation. The crystal
253 structures measured via Rietveld refinement of the powder X-ray diffraction pattern were used to
254 calculate molar mass. From the individual element balances between reactants within rock and products
255 within sediment, we estimated the scale and composition of the contribution of mineral derived cations
256 to subglacial water. Anion composition is constrained by the sulfur and carbon content of the source
257 rocks. This inferred fluid composition only includes elements weathered out of sampled tills.
258 Groundwater could conceivably add elements of an unquantified composition (Gooch et al., 2016).

259 From our closed system mass balance assumptions, we can calculate the input of atmospheric
260 gases necessary to perform the observed chemical weathering. The O_2 input is calculated indirectly from
261 the water composition under the assumption that the vast majority of the sulfate, bicarbonate, and
262 carbonate either inferred as dissolved solutes or precipitated as newly formed minerals was oxidized
263 from organic carbon and sulfite in the source rocks. This O_2 estimate in turn allows for an estimate of
264 meltwater input per g sediment from the known air content of ice (e.g. Gow and Williamson, 1975). The
265 estimate of meltwater input also constrains aerosol salt input to the subglacial system, which is also
266 known from ice cores (Legrand and Mayewski, 1997).

An erosion rate is required to convert the chemical mass changes and meltwater inputs per g sediment into fluxes. We employ a basal shear stress based model of subglacial sediment flux that includes Law Glacier (Golledge et al., 2013) and convert it to an erosion rate based on the surface area of the sediment supply catchment inferred from ice surface velocity (Rignot et al., 2011). We make an alternative flux estimate using long-term continent-wide denudation from the offshore record (Wilson et al., 2012). The former provides our estimate for our specific field site at Mt. Achernar Moraine. The latter provides an estimate for continent wide fluxes inasmuch as Mt. Achernar Moraine is representative of long-term continental averages.

Results

Representative Rocks (Baseline rock geochemistry)

The three igneous rock samples have broadly similar major and minor element abundances, with Rock 1 slightly more felsic and Rock 3 slightly more mafic (Figure 2a, Table S2). These differences are expressed by higher Ca and Mg, and lower Na and K in the more mafic rocks. Rock 1 is also enriched and Rock 3 depleted in the host of minor elements associated with felsic rocks (Table S3). The quantitative powder X-ray diffraction data show that all three samples are rich in plagioclase, with anorthite content varying from 62% in the most felsic sample to 70% in the most mafic sample (Table S4). The samples contain 21-37% clinopyroxene and 3-9% orthopyroxene. The more felsic samples are enriched in quartz and alkali feldspar; the more mafic samples are enriched in clinopyroxene. In the Rock 3, clinopyroxene is primarily pigeonite; in the others, clinopyroxene is primarily augite (Table S4). The most felsic sample (Rock 1) contains 4.4% smectite and 1% loss on ignition (LOI), reflecting the presence of secondary alteration products. Rock 2 has 3% smectite and 0.5% LOI (Figure 2d, Table S4). These abundances of secondary alteration products are also reflected in CH_3COOH extracted Fe (which varies from 0.7 wt. % in Rock 1 to 0.3 wt. % in Rock 3) (Table S6). HCl extracted Fe, Al, and Ca are 1-2

orders of magnitude more abundant in Rock 1 than in the other two dolerites, suggesting formation of oxyhydroxides in this sample only (Figure 2c). Rock 1 was striated and faceted by subglacial processes, possibly indicating it sourced from a more chemically active environment. Magnetic susceptibility varies from 1.33 wt. % magnetite equivalent in Rock 1 to 0.51 wt. % in Rock 3 (Figure 2d).

The sedimentary and meta-sedimentary rocks have substantially greater ranges in bulk compositions, especially for Si, Fe and Al, reflecting large variability in the abundance of quartz, feldspar, and clay minerals (Figure 2). Compared with igneous rocks, the (meta)-sedimentary rocks have, on average, 14.2 wt. % more Si, 2.2 wt. % more K, and 1.8 wt. % more LOI, balanced by 8.9 wt. % less Ca, 6.3 wt. % less Fe, and 4.5 wt. % less Mg (Table S2). Among minor elements, the sedimentary rocks are depleted in the period 4 transition metals compared to igneous rocks (lower values of Sc, Ti, V, Mn, Co, Ni, and Zn are statistically significant) (Table S3). The sedimentary rocks are enriched in most of the rest of the periodic table compared with the igneous rocks; enrichments in Ba, Sr, Zr, Ga, Rb, Nb, Cs, Hf, Ta, W, Tl, Pb, Th, U, and rare earth elements from La to Sm are statistically significant. Mineralogically, most of the sedimentary rocks contain some feldspar (mostly albite and K-feldspar), averaging 25% of the rock mass. Based on lack of separation within the ~23.6° 2θ (Cu) peak, we infer K-feldspar to be primarily orthoclase. Quartz ranges from 17-62% of the rock mass, with no discernable trend with respect to grain size (Figure 2). All samples except Rock 5 (sandstone) contained illite, with the highest clay abundances in the argillites and meta-sandstone (Figure 2). The two black argillites (Rocks 8 and 9) contained substantial chlorite (9 and 13% mass); 2-3% chlorite was found in four other samples (Figure 2d). The six chlorite-bearing rocks (Rocks 5-10) are also enriched in extractable Fe and Al (CH_3COOH, HCl, and NH_2OH-HCl extracts); the black argillites (Rocks 8 and 9) have the highest abundances (Figure 2, Tables S6-S8). Magnetic susceptibility in the sedimentary rocks varies from 0.08 – 1.61 wt. % magnetite equivalent, with a weighted average of 0.57 %; half the average of the igneous rocks (Figure 2c).

Our confidence in the representativeness of this data is boosted by past studies of the mineralogy of the bedrock of the central Transantarctic Mountains which have found broadly similar results to our rock clast characterizations. Assessment of 203 sedimentary rock samples from the Beacon Supergroup shows a broad range of composition, with most samples in the feldspathic graywacke range, i.e. 10-50% feldspar composition (La Prade, 1972). Zeolite phase alteration in the Beacon Supergroup, associated with the intrusion of Jurassic dolerites, shows similar zeolites (i.e. laumontite, clinoptilolite) to the sedimentary rock samples we analyzed (Bernet and Gaupp, 2005; Vavra, 1989). Clays in Beacon Supergroup rocks were similarly shown to be primarily of illite and chlorite composition, though the illite was described as sericite in earlier literature (Vavra, 1989).

The Ferrar Dolerite at Mt. Achernar has been directly analyzed for major element composition, and shows results similar to the three detrital sample we analyzed (Faure and Mensing, 2010). Past analyses of the Ferrar Dolerite have shown similar composition along the length of the Transantarctic Mountains (Elliot et al., 1999), suggesting that subglacial Ferrar Dolerite should be broadly similar to the surface exposed rock. Detailed mineralogical analyses at various sites have shown plagioclase feldspar to range from 50%-90% anorthite with most samples falling in the 62-75% anorthite range that we observe both in our three representative cobble clasts (Elliot et al., 1995) (Table S4). Past studies have shown that orthopyroxenes range from 50-80% enstatite and that clinopyroxenes vary broadly within augite and pigeonite compositional space (Elliot et al., 1995), also mirroring our observations from cobble clasts (Table S4).

Freshly Emerging Sediment Compared with Rock

Some of the chemical differences between sediment and cobble clasts are large enough that they are robust regardless of which method is used to characterize average rock composition. Freshly emerging sediment is 9.2 wt. % LOI, compared with 1.3-2.4 wt. % in the rock (Figure 2a). Magnetic

susceptibility is only 0.1 ± 0.02 wt. % magnetite equivalent, well below that found in either igneous or sedimentary rock averages (Figure 2c). There are also large changes in several of the minor elements across all three methods: Cr, Cu, Sb and Mo are substantially depleted in the sediment; Ti, Sr, Y, Zr, Ag, Cs, Hf and the rare earth elements are substantially enriched (Table S3). Some of these elements (i.e. Sb, Mo, Ag) are near detection limits and have variable reproducibility compared to reference standards (Table S3).

The pebble count method of comparison suggests that the <63 μm fraction contains more felsic minerals than the underlying rock. Major elements associated with mafic minerals (Fe, Ca, Mg) along with minor transition metals are significantly depleted; Si, Al and K and most other minor elements are significantly enriched (Figure 2a, Tables S2, S3). This pattern strongly suggests that the Ferrar Dolerite is preferentially preserved at the moraine surface and therefore enriched in the pebble counts. For this reason, the mass balance approach is a more accurate way to assess the average rock contribution to the <63 μm fraction in this setting.

The mass balance method assumes that an element is conserved in the system and that all rock types proportionately supply elements to the <63 μm fraction of the till. For rock abundance values to be positive, this requires that the element's abundance in the <63 μm fraction fall between that of igneous and sedimentary rocks. When normalized for the change in loss on ignition, Al, Ti, P, LOI, Sr, Y, Zr, Zn, Ga, Ge, Nb, Sn, Hf, Cs, Ta, Th, U, and the rare earth elements, are more abundant in the <63 μm fraction than either the sedimentary rocks or the igneous rocks (Tables S2, S3). Fe, Na, Cr, Cu, Mo, and W are depleted in the <63 μm fraction compared with either rock type. This leaves 13 elements where a mass balance analysis weighing contributions from igneous and sedimentary rocks is possible: Si, Mn, Mg, Ca, K, Sc, V, Co, Ni, Ba, Rb, Tl, Pb. The central tendency among these elements implies a contribution between 28 ± 7% igneous rock and 72 ± 7% sedimentary or metasedimentary rock to the freshly emerging sediment (Table S2, S3). These ratios of igneous to sedimentary rock were employed to

reweight the relative clast abundance for each of the two rock types. Unsurprisingly, changes in the elements used to calibrate the mass balance are not statistically significant (Tables S2, S3). Gains in P and Ti and losses in Fe, Na remain statistically significant (Table S2), along with many of the differences in minor element abundance (Table S3).

Mineralogical differences between rocks and freshly emerging sediments assessed through powder X-ray diffraction show large losses in feldspar and pyroxene content paired with increases in smectite, illite, and kaolinite content (Figure 2d). X-ray diffraction patterns of the isolated clay fraction also indicate changes in clay mineralogy between rock and subglacial sediment. The <63 μm fraction is dominated by smectites, which are only found in the igneous rocks (Figure 3). The smectite peaks in the sediments are also substantially broader than those of the igneous rocks, indicating greater disorder in layer stacking and/or multiple smectite fractions/compositions. The kaolinite peak shape in sediment approximately matches that found in igneous rock but at substantially greater abundance (Figures 2d, 3). The shales and argillites are dominated by illite and chlorite, which are found in comparable abundance and degree of order in the subglacial sediments (Figure 3). The gains in clay abundance, particularly smectite and kaolinite, are significant regardless of which method is used to assess average rock composition. However, the loss of plagioclase and pyroxene is substantially larger when pebble count approach is used (Figure 2d).

The H_2O extractable fraction is very small for both rock and freshly emerging sediments, although there is a slight increase in extractable salts relative to rock for even the freshest sediments (Table S5). The CH_3COOH extraction is dominated by Ca, presumably from the dissolution of $CaCO_3$. The fine sediment samples are enriched by ~0.6 wt. % CH_3COOH extractable Ca, compared with rock (Figure 2c). Freshly emerging fine sediment samples are also enriched in CH_3COOH extractable Na, and P compared with crushed rock, but the change (although statistically significant) is trivial (Table S6). CH_3COOH extractable K, Fe, and Al are depleted compared with rock. The HCl extraction was dominated

386 by Fe and Al, likely from dissolution of oxyhydroxides, as well as Ca, whose provenance is not
387 determined. Compared with rock, sediment is enriched in HCl extracted Al by 0.13 wt. %, and in HCl
388 extracted Ca by 0.22 wt. % (Figure 2c). HCl extracted Fe, P, Na, and K are less abundant in emerging <63
389 μm sediment than in rock by statistically significant values (Table S7). The NH_2OH-HCl extracted fraction
390 was dominated by Fe and Al. Freshly emerging sediment has a 0.56 wt. % increase in NH_2OH-HCl
391 extracted Fe and a 0.2 wt. % increase in NH_2OH-HCl extracted Al (Figure 2, Table S8). Small losses in Na
392 and Ca are statistically significant (Table S8). Magnetic susceptibility in the freshly emerging sediments is
393 0.61 wt. % magnetite equivalent lower than the weighted rock average (Figure 2c). This value is
394 comparable to the gain in NH_2OH-HCl extracted Fe.

395 In general, the compositional components isolated through sequential extractions align well
396 with the composition of the amorphous component as determined by bulk composition minus minerals
397 compositions and abundances identified through powder X-ray diffraction (Table S9). These two values
398 approximately align for Mg, Ca, Na, and K and we assume that the sequential extractions primarily
399 dissolved the amorphous components of the samples. For the <63 μm samples, sequentially extracted
400 Fe_2O_3 and Al_2O_3 exceeded the comparable components detected by X-ray diffraction by ~1 wt. % each.
401 For the rock samples, the opposite result is found, with the bulk weights of extracted Al and Fe being
402 less than the amorphous component determined by X-ray diffraction by ~1 wt. % each (Table S9). The
403 cause of these discrepancies is not clear.

404 The bulk composition / X-ray diffraction analysis of the sediment also identifies Si within in the
405 amorphous component and loss on ignition phases that were not analyzed by sequential extractions.
406 Sediment contains 10.05 wt. % amorphous Si and 4.7 wt. % amorphous loss on ignition, contrasting with
407 7.1 wt. % amorphous Si and 0.5 wt. % amorphous loss on ignition in the mass balance averaged rock
408 (Figure 2c, Table S9).

409

Interpretation of Sequential Extraction Data

The sequential extraction data provide quantitative data on elements soluble under specific extraction regimes. As an operationally defined procedure, the correspondence of these extractions to particular mineral phases is not fully resolvable (Tessier et al., 1979). The CH_3COOH extraction targets carbonate phases, and where calcite is sufficiently abundant to appear in the X-ray diffraction patterns, calcite abundances correspond closely with CH_3COOH extracted Ca (Tables S4, S6). However, most of the rock samples have large quantities of CH_3COOH extracted Fe (Table S6) that does not appear in the sediment samples and is unlikely to be associated with carbonate phases; Fe-carbonates were not detected by X-ray diffraction. We think the most likely explanation for the CH_3COOH extracted Fe is that the artificial comminution of the rock samples created new mineral surfaces with broken crystal surfaces ripe for chemical leaching. However, it's not clear the degree to which the artificial grinding caused the CH_3COOH extracted Fe to come from pools of Fe that would have otherwise been extracted later in the sequence or whether it represents extraction of Fe that would have otherwise remained in crystalline phases. The increase in NH_2OH-HCl extracted Fe in the sediment (Figure 2) would be entirely accounted for if the CH_3COOH extracted Fe actually comes from amorphous phases (and is not an artifact of the grinding processes). We cannot rule out that other extractions from the rock samples were also subject to artificial comminution effects.

The HCl and NH_2OH-HCl extractions are meant to target amorphous oxyhydroxides and poorly crystalline oxides respectively (Wiederhold et al., 2007), and are mostly expected to leach Fe and Al from those pools. However, substantial quantities of Ca are also leached in these phases, suggesting either further dissolution of carbonates or dissolution of silicates. A possible source for the HCl extracted Ca is zeolites whose abundance is below the XRD detection limits. Such zeolites are present in the clay mounts (Figure 3), but below detection in the whole rock samples. The molar abundances of the increases in HCl extracted Ca, extractable Al, and Si were measured at approximately a 1:2:4 molar ratio

(Table S10), similar to that of many zeolites. Such zeolites have been previously been documented as cement of Antarctic tills (Dickinson and Grapes, 1997). However, other amorphous species such as allophane, opal, etc., may also be newly formed in the subglacial environment. And, other explanations, including clay dissolution or cation exchange, cannot be ruled out.

Mineral Balance between Freshly Emerging Rock and Sediment

The total mineral abundances in the disaggregated portion of the subglacial sediment (including monomineralic sand) is estimated via Equation 1 and compared with the average mineral abundance in rock (Figure 4). Mass balance assuming illite conservation, produces a sand fraction with 51% polymineralic, lithic fragments (Table S10). Light microscope examination of sand from 5 samples shows a sharp contrast at ~500 μm, with larger grains almost exclusively polymineralic, lithic grains and smaller grains predominately monomineralic. At first order, this is consistent with the mass balance estimate of the lithic fragment percentage. Employing the mass balance average for rock composition, per g sediment, the average sediment is short 230 ± 35 μmoles of plagioclase feldspar, 60 ± 73 μmoles of albite, 113 ± 10 μmoles of orthoclase, and 188 ± 49 μmoles of pyroxene compared with average rock. These losses are balanced by an increase of 220 ± 100 μmoles of smectite and 80 ± 76 μmoles of kaolinite (Figure 4, Table S10). Increases in HCl and NH_2OH-HCl extracted Al imply 129 ± 63 μmoles of Al within amorphous or poorly crystalline material newly formed in the sediment. CH_3COOH extractable Ca represents 154 ± 58 μmoles, assumed to speciate as calcite; HCl extractable Ca represents 44 ± 35 μmoles. The relative loss of pyroxene and feldspar suggests that 56% of the newly formed smectite is Al-bearing (i.e. beidellite or montmorillonite) and 44% is Fe- or Mg-bearing (e.g. saponite). Amorphous Si represents 153 ± 475 μmoles. The total change in mineral balance requires gains in clays, carbonates, and other extractable compounds in the till (Figure 4).

457 Assuming the amorphous and extractable phases represent a pool of chemical weathering
458 precipitates that are distinct from the clay minerals (Table S9), the loss of rock-forming minerals
459 between cobble sized clasts and fine sediment requires 929 ± 156 μ equivalents of cations released
460 during mineral dissolution (i.e. Figure 4). Ca delivery to the CH_3COOH extractable and HCl extractable
461 pools accounts for 397 ± 95 μ equivalents. The cations in smectite interlayers represent 84 ± 44 μ
462 equivalents. This leaves 447 ± 216 μ equivalents per g of cation material lost to subglacial fluid. Based on
463 the composition of the weathering material, the composition of this fluid per g of sediment includes 100
464 ± 75 μmoles of Na, 112 ± 10 μmoles of K, 35 ± 81 μmoles of Ca, and 82 ± 61 μmoles of Mg (Table S10).
465 Loss of Si and Fe to the dissolved fraction is also substantial (Figure 4, Table S10). Our assumptions of no
466 weathering within lithic fragments, sand composition equal to silt, illite conservation between rock and
467 sediment, and mass balance approach to average rock composition all introduce errors not expressed
468 within the analytic uncertainties. Several of these assumptions (i.e. lithic fragments, mass balance
469 approaches) minimize the total chemical weathering.
470 The total of 447 ± 216 μ equivalents of cations lost to water in the weathering of rock minerals
471 (Figure 4) requires a comparable release of anions by chemical weathering. Likewise, the CH_3COOH
472 extractable Ca requires a source of carbonate to form calcium carbonate as a product of carbonic acid
473 weathering. Including carbonate precipitation, 763 μ equivalents of anions per gram sediment are
474 needed. The plausible pathways for anion generation are the oxidation of Fe sulfides, producing sulfate
475 as a product of sulfuric acid weathering, and the oxidation of organic carbon, producing bicarbonate or
476 carbonate as a products of carbonic acid weathering. Carbon and sulfur wt. % values have been reported
477 for rocks of the Ferrar Dolerite and Beacon Supergroup collected elsewhere. In the Permian sedimentary
478 rocks that underly Mount Achernar Moraine, average organic matter content in unaltered rock samples
479 ranges from 0.55 wt. % in the Mackellar Formation to 23 wt. % in the coal-bearing Buckley Formation
480 (Horner, 1992). Through most of the sedimentary rock section, sulfur content is <200 ppm. However,

481 the Lower Buckley Formation has coal-rich lenses where sulfur values are as high as 2,500 ppm,
482 concurrent with total organic matter content of >50% mass (Horner, 1992). At Tillite Glacier (~100
483 kilometers down ice flow from our field site), Ferrar Dolerite sulfur contents range from 100 to 600 ppm
484 (Faure and Mensing, 2010). These data suggest that taking igneous and sedimentary rock together, the
485 sulfur content of the rock substrate of the Mt. Achernar moraine is unlikely to be more than 600 ppm,
486 which when corrected for molar mass, would amount to <20 micromoles S per gram sediment. Even if
487 this were fully oxidized to sulfuric acid, it would account only 40 out of 763 µmoles of the acid content
488 needed to form the alteration product content observed in the glacial tills. If the remaining acid came
489 entirely from carbonic acid, ~725 micromoles of carbonic acid derived alkalinity per g are needed to
490 drive the observed alteration of rock-forming minerals. 154 ± 58 micromoles of C are within the calcium
491 carbonate precipitates found in the freshly emerging till (i.e. the CH_3COOH extraction – fig 2), providing
492 ~300 micromoles of the necessary alkalinity. Assuming the non-precipitated carbon anions remained as
493 aqueous bicarbonate, a total of 575 ± 224 micromoles of carbon per gram sediment is implied. If this
494 were predominately oxidized from organic carbon, the source rocks would need total organic carbon
495 values of at least 0.7 ± 0.3 wt. % mass. This value is within the range found in the Beacon Supergroup
496 sedimentary rocks, even accounting for an ~30% input from Ferrar Dolerite.
497
498 *Erosion Rate and Total Chemical Flux*
499 In order to convert chemical weathering per g sediment into a chemical drawdown rate, we
500 need to estimate the erosion rate at the site. Golledge and others' (2013) model of sediment flux as a
501 function of basal shear stress suggest that down-glacier sediment flux across Law Glacier at Mt.
502 Achernar moraine is on the order of 1 m^3 sediment per glacier cross-section m per year (Figure 5). Ice
503 surface velocities indicative of basal shear capable of sediment transport begin ~100 km up glacier from

Mt. Achernar Moraine (Rignot et al., 2011), suggesting a sediment catchment area on the order of ~4000 km^2 (Figure 5).

Using a 1 $m^3 \cdot m^{-1} \cdot yr^{-1}$ sediment flux rate through the 25 km width of Law Glacier, a subglacial till density of 2 $g \cdot cm^{-3}$, and a 4000 km^2 sediment catchment area (i.e. Figure 5), we infer an approximate erosion rate for the sediment catchment of Mt. Achernar Moraine of 12.5 $g \cdot m^{-2} \cdot yr^{-1}$. This model result is highly comparable to the sediment accumulation rate inferred at Mt. Achernar moraine, which accumulates 12.4 $g \cdot m^{-2} \cdot yr^{-1}$ if surface till density is assumed at 1.8 $g \cdot cm^{-3}$ (Graly et al., 2018b). If the density of the underlying rock is 2.7 $g \cdot cm^{-3}$, this is equivalent to a time-averaged denudation rate of 4.6 $m \cdot Ma^{-1}$. Based on our calculated carbon oxidation mass per g sediment of 0.7 ± 0.3%, this erosion rate gives a CO_2 drawdown rate of 0.33 ± 0.14 $g \cdot m^{-2} \cdot yr^{-1}$ for the Mt. Achernar basin. This erosion rate is consistent with the relatively small ice flux through the Law Glacier outlet. If we alternatively use modeled erosion rates averaged for the entire East Antarctic Ice Sheet from the Oligocene to the present, which are on the order of 15-25 $m \cdot Ma^{-1}$ (Wilson et al., 2012), 1.40 ± 0.35 $g \cdot m^{-2} \cdot yr^{-1}$ of CO_2 drawdown is inferred.

Inferred Water Flux and Sediment Residence Time

To oxidize the estimated levels of carbon and sulfur into carbonic and sulfuric acid, ~600 micromoles of O_2 are needed per g sediment. Although, in principle, some of the oxidation could occur through the reduction of a multi-valent metal, there is no evidence of such oxidation-reduction coupling in the data we present. In particular, the decline in magnetism between the rock and subglacial sediment and the commensurate increase in NH_2OH-HCl extracted Fe (Figure 2) strongly suggest that Fe is also being oxidized in the system. None of the other redox capable metals (e.g. Mn, Co, Cu, etc.) occur at anywhere near the abundance necessary to be a substantial source of O_2 (Table S3). During formation, Antarctic ice traps ~12 cm^3 of air per 100 g of ice (Gow and Williamson, 1975). Given the

density of air and ice and partial pressure of oxygen, this is equivalent to ~1 micromole O_2 per cm^3 of ice. Thus, in a subglacial system closed to contact with the atmosphere, ~600 cm^3 of ice per g sediment would have to be delivered as basal melt to produce the chemical alterations we infer. Analyses of Antarctic subglacial tills elsewhere give densities of ~2 $g \cdot cm^{-3}$ and porosities of ~0.4 (Tulaczyk, 1999), suggesting ~0.2 ml H_20 per g sediment. Using these values and correcting for the density of ice, the meltwater required to supply the inferred level of O_2 would fill the pore space around the sediment ~2700 times, or 543 ± 201 ml meltwater per g sediment (Figure 6, Table S10). This would require water to be cycled through the system more than three orders of magnitude faster than sediment, even as basal melt delivers water to the system at rates of less than 1 cm per year (Pattyn, 2010).

Discussion

Subglacial Alteration Processes

Three processes can affect bulk chemical and mineralogical differences when comparing subglacial fine sediment with the underlying bedrock: 1) Physical processes can preferentially grind one mineral or rock type into fine sediment (Sharp and Gomez, 1986); 2) Chemical processes can dissolve minerals, producing weathering products such as solutes, clays, oxides and oxyhydroxides (Graly et al., 2016; Tranter et al., 2002); and 3) Subglacial water can preferentially transport sediment of a certain grain size within the subglacial system (Alley et al., 1997). Each of the elements and mineral species enriched in the fine sediment must be formed or concentrated by one of these processes. Because we measured the <63 µm fraction in contrast to cobble clasts, we assume that preferential comminution (1) plays a large role in the chemical and mineralogical differences we observe. And we normalize the data with illite conservation (Eq.1, Figure 4) to minimize newly formed clay minerals and thereby maximize the role of comminution in our model. However, the following changes are far too large to be explained by these grain size sorting processes: the 15-fold increase in smectite clay, the 7-fold increase in

552 kaolinite clay, and the 6-fold increase in calcite as CH_3COOH extractable Ca (Figure 4; Tables S4, S6).
553 Comparably, the 50% decline in abundance for feldspar and pyroxene in the <63 μm fraction cannot be
554 explained by a preference of these minerals for larger grain sizes, especially when quartz, which is a less
555 friable mineral (Sharp and Gomez, 1986), shows a smaller decline. We must either infer selective
556 transport of clay and calcite into the subglacial environment supplying sediment to Mt. Achernar
557 moraine (3) or conclude that the clay minerals and calcite formed *in situ* (2) from the weathering of the
558 pyroxene and feldspar and the saturation precipitation of carbonate minerals (i.e. Figure 4). The
559 glaciology at the Mt. Achernar site suggests insufficient water in the subglacial system to mobilize
560 subglacial sediment or cause grain size sorting. We therefore consider the mass conservative, chemical
561 weathering approach employed in our analysis to best explain the data presented.

562 Within a mass conservative system, chemical differences between rock and the <63 μm fraction
563 of the sediment must either be explained by preferential comminution of certain minerals into the <63
564 μm fraction, preferential precipitation of elements from those minerals into newly formed minerals
565 within the <63 μm fraction, or preferential leaching of those elements into out-fluxing water. For a wide
566 range of rare earth and trace elements, the increase in their abundance in <63 μm sediment compared
567 with rock is too large to be explained by mass loss to the solute fraction alone (Figure 2b, Table S3).
568 Either small initial crystal sizes that disaggregate into the fine fraction or preferential comminution of
569 minerals bearing these elements is the most likely explanation. Al is the only major element associated
570 with primary rock-forming minerals that is enriched in the <63 μm fraction. This likely reflects
571 disaggregated and newly precipitated Al-rich clays found only in the <63 μm fraction. Our mineral
572 balance suggests that Si, Fe, Mg, Ca, Na, and K are chemically leached from the system (Figure 4, Table
573 S10). Of these, only Na and Fe are depleted in the <63 μm fraction (Figure 2). For Na, this is likely
574 because it is largely excluded from clay interlayers, carbonates, and zeolites, which precipitate in the
575 fine fraction. The depletion of Fe in the <63 μm fraction is more difficult to explain. Physical preference

against comminution of Fe-rich minerals would also affect Ca and Mg, for which such effects are not observed (Figure 2). Fe is no more chemically leached than any other major element. The sedimentary rocks included in this analysis have highly variable Fe abundances (Figure 2), due to high amorphous Fe oxide and oxyhydroxide content in some of the shales and argillites. It is possible that our calculation of Fe abundance in the sedimentary rocks is therefore skewed by outlier samples. With the entire range of elements and minerals considered, we have strong evidence of both preferential comminution of minerals into the <63 μm fraction and chemical leaching at the Mt. Achernar site.

The fundamental hydrology of the East Antarctic subglacial environment does not favor physical sorting of grains by subglacial water. Subglacial water under the East Antarctic Ice Sheet has been observed and modeled to occur in lakes and as groundwater between lakes (Siegert et al., 2018; Wright and Siegert, 2012). The catchment of Law Glacier, together with several other outlet glaciers of the Transantarctic Mountains, has small lakes (i.e. <0.1 km^3) in the subglacial environment (Smith et al., 2009). The steep surface slopes or seasonal fluctuations that support sediment transport via large flow through subglacial conduits (Alley et al., 1997) do not exist in this setting. Rapid subglacial lake drainage events have been observed in some settings and would cause flows capable of mobilizing subglacial sediment (Wingham et al., 2006), but with limited spatial and temporal extent.

Physical transport of clays in the subglacial environment is a highly unlikely explanation for clay enrichment at our site. During the rare lake drainage event, flowing water would primarily winnow away fine particles. For clay minerals to be enriched at Mt. Achernar Moraine by physical means, clay-sized particles winnowed elsewhere would have to be preferentially deposited in the subglacial environment delivering sediment to Mt. Achernar moraine. No evidence of such sorting exists in the emerging till. Clay- to car-sized boulders emerge in the same debris bands, indicating a lack of sorted sediment in the subglacial environment. The isotopic signature of the ice entraining the debris is consistent with a regelation enrichment process occurring at the glacier bed (Graly et al., 2018c), which provides a

mechanism for sediment entrainment into a till bed without grain size discrimination (Iverson and Semmens, 1995; Rempel, 2008). Finally, the enrichment in clay mineral content with respect to rock is fairly uniform along the length of the moraine, with samples up to 12 km apart showing comparable clay content (Figures 1, 2d). In contrast, the deposition of clays winnowed from elsewhere depends on very low flow conditions and is likely to be a heterogeneous process. In sum, we find our mass conservative assumptions robust against considerations of grain-size selective transport within the regional subglacial system.

Ice Melt Budget for the Subglacial Environment

The erosion rate for the Law Glacier catchment inferred from Golledge and others' (2013) model balances very closely with the estimated input of O_2 inferred by our closed system assumptions. If we assume steady and uniform loss of sediment from the catchment, 7400 $cm^3 \cdot m^{-2} \cdot a^{-1}$ of ice would have to melt to obtain the oxidation balance implied by the rate of chemical weathering, creating a basal melt rate 7.4 mm per year (Figure 6, Table S10). Modeling suggests basal melting on the order of 5-10 $mm \cdot yr^{-1}$ in the region of the Law Glacier catchment area (Figure 5) (Pattyn, 2010). Thus, independent models of basal melt (Pattyn, 2010) and sediment generation (Golledge et al., 2013) suggest three orders of magnitude greater rates of water cycling than sediment cycling in the catchment of Mt. Achernar Moraine, consistent with the budget of oxygen and carbon that we infer by comparing rock composition with freshly emerging subglacial sediments. If we knew the thickness of the actively weathering subglacial sediment, we could extrapolate from a basal melt rate to a sediment residence time. For instance, a basal melt rate of 7.5 mm per year and an active subglacial sediment thickness of 1 m would give a sediment residence time of 160,000 years, whereas saturated porewater under these conditions would have a residence time of only ~60 years.

623 Despite the support of model results for these rates of chemical cycling, there are alternative
624 explanations for the balance of weathering products that would lead to substantially different
625 interpretations of water and O_2 cycling. A substantial component of the CO_2 that forms carbonic acid
626 could source from fermentation of organic matter, which produces CO_2 and CH_4 in an anoxic
627 environment (Wadham et al., 2012). This requires twice as much organic matter consumption but still
628 could be within the range of organic carbon concentrations found in Beacon Supergroup rocks. If this is
629 the case, then the same observed level of chemical weathering per g sediment could occur with
630 substantially lower basal melt rates, limited only by the abundance of organic matter in the system.
631 We also presently cannot rule out an inherited weathering signal from a preglacial (e.g.
632 Miocene) or Pliocene period of surface exposure, which would imply a portion of the chemical
633 weathering occurred when the material was in direct contact with the atmosphere. Smectite and
634 kaolinite minerals are observed in regions of Antarctica that have never been covered by ice (Vennum
635 and Nejedly, 1990). However, at least under present environmental conditions, these remain at very low
636 abundances (<1 wt. %). Furthermore, the smectite clays are described as highly ordered (Vennum and
637 Nejedly, 1990), resembling what we observe in samples of underlying rock and not the subglacial
638 sediments (Figure 3). If soil minerals are inherited from pre-glacial exposure, it represents a time in the
639 Antarctica's deep past, where thick, clay-rich saporlite formed under environmental conditions very
640 different from present. We find it unlikely that such material would have survived the intervening tens
641 of millions of years of erosive forces.
642
643 *Implications for the Offshore Record*
644 Analyses of the clay minerals in Antarctic offshore cores have long been interpreted as recording
645 climatic information. The preglacial clay mineral assemblages from the Eocene have >90% smectite (and,
646 in some cases, kaolinite), consistent with intensively weathered material being delivered to the marine

environment (Ehrmann et al., 1992), although some of the smectite may have formed authigenically in the marine environment (Ehrmann et al., 2005). The onset of glaciation in the Oligocene is concurrent with a rapid rise of offshore illite and chlorite; typical glacial-era assemblages contain ~50% illite, ~30% smectite, ~10% chlorite, and ~10% kaolinite (Ehrmann et al., 1992). These glacial-era assemblages closely match the relative clay mineral abundances that we observe in the freshly emerging fine sediment of Mt. Achernar Moraine. Detailed analyses of the degree of layer stacking order and composition of the offshore clay minerals show that glacial-era smectite is more disordered (i.e. broader X-ray diffraction peaks) and is more Al-rich (less Fe/Mg rich) than preglacial clays (Ehrmann, 2001; Ehrmann et al., 2005; Setti et al., 2004). The morphology of poorly ordered smectite, as seen in SEM images, is consistent with a non-authigenic origin and attributed to non-glacial volcanic input (Ehrmann et al., 2005). However, our recognition of smectite formed in the subglacial environment, which could then be detrital in the offshore environment, presents an alternative source of these offshore clays. The offshore smectites and the smectites analyzed here are similar in degree of order (i.e. Figure 3) and similarly Al-rich (i.e. Table S10). We therefore suspect that subglacially formed smectite subsequently transported to the marine environment could be a major component of offshore smectite during glacial periods.

Solute Composition and Flux Compared with Existing Measurements

The subglacial water composition inferred from the mineral mass balance can be compared with measurements of subglacial water compositions collected elsewhere on the Antarctic continent, thereby putting our observations into the context of direct chemical weathering observations. Subglacial water samples have been collected at Subglacial Lake Whillans (Christner et al., 2014; Michaud et al., 2016) and in the till porewaters beneath the Kamb and Bindschadler ice streams (Skidmore et al., 2010). A jökullhaup event near Casey Station, East Antarctica in 1985 and 1986 allowed for sampling of what had

likely been stored subglacial water (Goodwin, 1988). As a permanently ice-covered proglacial lake, Lake Untersee, Dronning Maud Land, has a chemical composition primarily influenced by input of subglacial water into the lake (Wand et al., 1997). The lake is chemically stratified with a thin (<20 m) surface-water layer containing most of Lake Utersee's sulfate. Upwelling subglacial brines at land terminal margins have been characterized at Lewis Cliff Ice Tongue (Fitzpatrick et al., 1990; Liu et al., 2014; Sun et al., 2015) and Blood Falls (Badgeley et al., 2017; Mikucki et al., 2004).

The major ions measured at these diverse Antarctic sites span a very wide compositional range, especially for anions (Figure 7). Unless there is a source of sulfate or chlorine (e.g. from groundwater) in the system that we have not identified, the sulfur and carbon abundances in the underlying rock suggest bicarbonate is the dominant anion in the system at Mt. Achernar Moraine, resembling the bottom waters of Lake Untersee more than any other site. The cation composition is also comparable to the bottom waters of Lake Untersee, but is within the range of values from the ice stream porewaters as well as Blood Falls. The largest difference between the inferred Mt. Achernar Moraine and most observed Antarctic water compositions is the input of brine or seawater at other sites. Geology probably exerts some control on these compositions, as the pyroxene and plagioclase feldspar that dominate the loss to chemical weathering at Mt. Achenar (Figure 2) may not be present at every site. Likewise, the underlying presence of sulfide or organic carbon for oxidation would control the anion composition. Water and sediment residence times likely also play a role (Graly et al., 2018a). The similarity to Lake Untersee suggests commonality between Mt. Achernar Moraine with other Antarctic sites where brine formation is minimal.

The CO_2 drawdown rate inferred at Mt. Achernar moraine is the first such calculation for the Antarctic subglacial environment and can be compared to data sets from elsewhere on Earth (Figure 8). Data from the world's major river basins and volcanic islands suggest a value of 4.3 $g \cdot m^{-2} \cdot yr^{-1}$ as the global average CO_2 drawdown through silicate weathering in the world's riverine landscapes more than

order of magnitude larger than the 0.33 ± 0.14 $g \cdot m^{-2} \cdot yr^{-1}$ we estimate for Mt Archernar Moraine (Gaillardet et al., 1999). The Mt. Achernar Moraine CO_2 drawdown value is equivalent to those found in arid regions of cratonic land masses, which represent the low end of silicate weathering CO_2 drawdown rates in the Gaillard et dataset (Figure 8). However, if we employ the long term average denudation rate for the East Antarctic Ice Sheet to calibrate CO_2 drawdown, our value of 1.40 ± 0.35 $g \cdot m^{-2} \cdot yr^{-1}$ is equivalent to silicate weathering CO_2 drawdown rates found in the highest latitude river basins in the Gaillardet dataset (Figure 8).

Other ice flow catchments of Antarctic outlet glaciers have substantially larger sediment fluxes than Law Glacier (Golledge et al., 2013), potentially suggesting far larger rates of chemical cycling in the continent's largest ice streams. However, we would only expect chemical weathering rates to scale to sediment flux if chemical weathering under Antarctica is sediment supply limited. Inasmuch as the primary factor limiting chemical weathering in the Antarctic subglacial system is basal melt and the consequent supply of O_2 to meltwater, Law Glacier, with a basal melt rate around that of the continent average (Pattyn, 2010), may be a fairly representative study site. Furthermore, it is likely that most of the CO_2 drawn down under Antarctic ice originates as organic carbon, whereas the bicarbonate in rivers that sources from silicate weathering reactions primarily contains CO_2 of atmospheric origin (Petsch, 2014). Further work is needed to determine the representativeness of our field site and confirm the inferred rates of water and sediment cycling.

Conclusions

Subglacial sediments freshly emerging at Mt. Achernar moraine are chemically weathered compared with cobble clasts representative of underlying bedrock. This is evidenced by large increases in the smectite and kaolinite content of the subglacial sediment relative to rock. Although smectite exists in the underlying rock, rock-bound smectite has greater layer stacking order and occurs in far

lower abundance than what is found in freshly emerging subglacial sediments. Carbonates, zeolites, and amorphous or poorly crystalline oxides detected by acid-leachable Ca, Fe, and Al also have higher abundance in glacial sediments. The total balance of mineral species between rock and sediment suggests that observed sediment chemical weathering products could have formed entirely from mineral material found in rock, without need for selective addition or removal of mass from the subglacial system by physical means. Independent models of basal melt and sediment flux at the site suggest that the gases released from melting basal ice over the sediment residence time would supply sufficient oxygen to form the carbonic and sulfuric acid necessary to perform the weathering reactions indicated by the mineralogical changes. These data, together with a growing body of evidence collected elsewhere on the Antarctic continent, suggest that chemical alteration in Antarctica's subglacial environment occurs on a scale that is likely to be significant for global geochemical cycles.

Acknowledgements

This paper was edited by A. Dosseto and thoughtfully reviewed by R. Rudnick and two anonymous reviewers. This work was supported by National Science Foundation Antarctic grants PLR-1443433, PLR-1443213, ANT-0944578 and ANT-0944475, by an Indiana University Collaborative Research Grant, and by funding from the IUPUI Office of the Vice Chancellor for Research. The US Antarctic Program, Kenn Borek Air, Ltd., and field team members from the 2010 and 2015 seasons are gratefully acknowledged for their support, particularly M. Kaplan. T. Kennedy assisted with magnetic susceptibility analyses. H. Johnston assisted with particle size analyses. S. Cox and S. Olund assisted with the sequential extraction analyses. We would like to acknowledge the Integrated Nanosystems Development Institute (INDI) for use of their Bruker D8 Discover X-ray diffraction instrument, which was awarded through NSF grant MRI-1429241.

Figure Captions

Figure 1: Sampling locations for freshly emerging sediment on Mt. Achernar Moraine, Central - Transantarctic Mountains. Approximate flowlines on Law Glacier are illustrated both down glacier and into the moraine (Kassab et al., 2020). Digital Globe imagery (©2014) provided by the Polar Geospatial Center (St. Paul, Minnesota, USA)

Figure 2: Abundance of selected elements, minerals, and amorphous phases in rock compared with the fine fraction of emerging subglacial sediments. For each element or phase, the first column shows igneous rocks (n=3), the second column shows sedimentary and metasedimentary rocks (n=9), and the third column shows freshly emerging sediments (black triangles) compared with two methods of averaging rocks (red and yellow stars). The clast-count average uses the raw abundance of each rock type on the freshly emerging moraine surface, where mafic igneous rocks (Ferrar dolerite) make up 62% of the rock clasts, and (meta) sedimentary rocks comprise 38% (Beacon Supergroup). The mass balance average reweights these abundances so that igneous rock accounts for 28% and (meta) sedimentary rock accounts for 72% of the underlying material.

Figure 2 continued

Figure 3: Selected peaks and patterns from X-ray diffraction patterns of clay mineral isolates, rescaled for peak comparison. A) Patterns for air-dried and ethylene glycol-saturated for clays isolated from <63 µm sample 1A; patterns from other <63 µm sediment samples are nearly identical. B) Smectite peaks from <63 µm air-dried sediment (1A) compared with those found in the igneous rock (Rock 1); note that the smectite peak is far broader in the sediment sample than in the rock sample. C) Ethylene glycol-saturated samples of the same. D) Illite and zeolite peaks in <63 µm sediment (1A) compared with typical sedimentary rocks. The peak shape found in the Rock 4 clay sample is also found in the clay mounts from rocks 7, 9, 10, and 12; the peak shape from rock 6 is also found in rock 11. Rock 5 is the only clay mount from rock with a detectable laumontite peak; laumontite is detected in all <63 µm sediment samples. The clinoptilolite peak observed at 9.6˚ in the <63 µm sediment samples is not present in any of the analyzed rocks. E) Kaolinite and chlorite peaks from <63 µm sediment compared with a chlorite peak from sedimentary rock (Rock 9 – other rocks similar) and a kaolinite peak from igneous rock (Rock 1); the glacial sediment peak integrates the two.

Figure 4: The balance of mineral content between subglacial sediment and the underlying rock highlighting the subglacial transformation. A) The proportion of the rock minerals that alter to form the new secondary products in sediment are indicated by the flow of material into the box labeled authigenic contribution. The glacial sediment is significantly enriched in smectite and kaolinite, calcite, and amorphous products, which are labeled as products of the authigenic contribution. Water and oxygen from ice melt also add mass to the authigenic contribution and mass is lost into dissolved solids. B) The authigenic contribution is broken down by element. Height scales to mass in weight % of each element dissolved or precipitated into each fraction.

Figure 5: Estimate of the approximate Mt. Achernar moraine sediment catchment area imposed on models of A) surface velocity (Rignot et al., 2011), B) basal melt (Pattyn, 2010), and C) sediment flux (Golledge et al., 2013). The catchment for Law Glacier above the Mt. Achernar moraine is delineated with a dashed line in A and B. The moraine is marked with a star in C.

Figure 6: Conceptual sketch illustrating fluxes relevant to the subglacial system at Mt. Achernar Moraine. The ice column values are from ice core studies (Gow and Williamson, 1975; Legrand and Mayewski, 1997). The sediment flux reflects results from a model of down glacier sediment shear as a function of surface velocity (Golledge et al., 2013) as well as the sediment accumulation rate for Mt. Achernar moraine (Graly et al., 2018b). The total O_2 load in the sediment is from our mass balance calculations (Figure 4, Table S10). The melt rate value reflects model results (Pattyn, 2010) as well as balance between the O_2 load and the sediment flux. All values are approximate.

Figure 7: A Piper diagram comparing geochemical results for Antarctic emerging and subglacial waters with the inferred subglacial water composition at Mt. Achernar Moraine based on the mineral balance between rock and <63 μm sediment. The chemical weathering regime in the source regions for Mt. Achernar Moraine appears similar to that observed at Lake Untersee.

Figure 8. Rate of alteration of CO_2 into calcite or bicarbonate at Mt. Achernar moraine compared with the CO_2 drawdown caused by silicate weathering in representative large river basins (Gaillardet et al., 1999). The two Mt. Achernar values were derived using the erosion rate implied from sediment flux estimates past Mt. Achernar moraine and an estimated catchment size (Fig. 5) (Local Catchment) and from an estimate for average Quaternary erosion rate for the entire East Antarctic Ice Sheet (Wilson et al., 2012) (Continent Average). These are compared with the five highest latitude rivers in the Gaillardet dataset, their global average estimate, and the minimum value from the Gaillardet dataset, which was obtained from the Zambese River.

Table Titles

Table S1. Sample location, descriptions, and analyses performed

Table S2. Major element concentrations in bulk sediment and rock samples

Table S3. Trace element concentrations in bulk sediment and rock samples

Table S4. Powder X-ray diffraction and Rietveld refinement results.

Table S5. Water extraction results

Table S6. Acetic acid extraction results.

Table S7. HCl extraction results.

Table S8. Hydroxylamine HCl extraction results.

Table S9. Amorphous compositions from bulk composition and X-ray diffraction

Table S10. Mineral Balance between rock and sediment

References Cited

Alley, R. B., Cuffey, K. M., Evenson, E. B., Strasser, J. C., Lawson, D. E., and Larson, G. J., 1997, How glaciers entrain and transport basal sediment: physical constraints: Quaternary Science Reviews, v. 16, p. 1017-1038.

Anderson, S. P., Drever, J. I., and Humphrey, N. F., 1997, Chemical weathering in glacial environments: Geology, v. 25, no. 5, p. 399-402.

Bader, N. A., Licht, K. J., Kaplan, M. R., Kassab, C., and Winckler, G., 2017, East Antarctic ice sheet stability recorded in a high-elevation ice-cored moraine: Quaternary Science Reviews, v. 159, p. 88-102.

Badgeley, J. A., Pettit, E. C., Carr, C. G., Tulaczyk, S., Mikucki, J. A., and Lyons, W. B., 2017, An englacial hydrologic system of brine within a cold glacier: Blood Falls, McMurdo Dry Valleys, Antarctica: Journal of Glaciology, v. 63, no. 239, p. 387-400.

Barrett, P. J., Elliot, D. H., and Lindsay, J. F., 1986, The Beacon Supergroup (Devonian-Triassic) and Ferrar Group (Jurrasic) in the Beardmore Glacier Area, Antarctica: Geology of the central Transantarctic Mountains, v. 36, p. 339-428.

Bernet, M., and Gaupp, R., 2005, Diagenetic history of Triassic sandstone from the Beacon Supergroup in central Victoria Land, Antarctica: New Zealand Journal of Geology & Geophysics, v. 48, p. 447-458.

Bintanja, R., 1999, On the glaciological, meteorological, and climatological significance of Antarctic blue ice areas: Reviews of Geophysics, v. 37, no. 3, p. 337-359.

Bish, D. L., and Post, J. E., 1989, Modern Powder Diffraction, Mineralogical Society of America Reviews in Mineralogy, Volume 20, p. 369.

Chadwick, O. A., Brimhall, G. H., and Hendricks, D. M., 1990, From a black to a gray box—a mass balance interpretation of pedogenesis: Geomorphology, v. 3, no. 3-4, p. 369-390.

Christner, B. C., Priscu, J. C., Achberger, A. M., Barbante, C., Carter, S. P., Christianson, K., Michaud, A. B., Mikucki, J. A., Mitchell, A. C., Skidmore, M. L., Vick-Majors, T. J., and WISSARD, S. T., 2014, A microbial ecosystem beneath the West Antarctic ice sheet: Nature, v. 512, p. 310-313.

Crompton, J. W., Flowers, G. E., Kirste, D., Hagedorn, B., and Sharp, M. J., 2015, Clay mineral precipitation and low silica in glacier meltwaters explored through reaction-path modelling: Journal of Glaciology, v. 61, no. 230, p. 1-18.

Dickinson, W. W., and Grapes, R. H., 1997, Authigenic chabazite and implications for weathering in Sirius Group diamictite, Table Mountain, dry valleys, Antarctica: Journal of Sedimentary Research, v. 67, no. 5, p. 815-820.

Ehrmann, W., 2001, Variation in smectite content and crystallinity in sediments from CRP-3, Victoria Land Basin, Antarctica: Terra Antartica, v. 8, no. 4, p. 533-542.

Ehrmann, W., Setti, M., and Marinoni, L., 2005, Clay minerals in Cenozoic sediments off Cape Roberts (McMurdo Sound, Antarctica) reveal palaeoclimatic history: Palaeogeography, Palaeoclimatology, Palaeoecology, v. 229, p. 187-211.

Ehrmann, W. U., Melles, M., Kuhn, G., and Grobe, H., 1992, Significance of clay mineral assemblages in the Antarctic Ocean: Marine Geology, v. 107, no. 4, p. 249-273.

Elliot, D. H., Fanning, C. M., Isbell, J. L., and Hulett, S. R. W., 2017, The Permo-Triassic Gondwana sequence, central Transantarctic Mountains, Antarctica: zircon geochronology, provenance, and basin evolution: Geosphere, v. 13, no. 1, p. 155-178.

Elliot, D. H., Fleming, T. H., Haban, M. A., and SIders, M. A., 1995, Petrology and mineralogy of the Kirkpatrick Basalt and Ferrar Dolerite, Mesa Range Region, North Victoria Land, Antarctica, *in* Elliot, D. H., and Blaisdell, G. L., eds., Contributions to Antarctic Research IV, p. 103-141.

878 Elliot, D. H., Fleming, T. H., Kyle, P. R., and Foland, K. A., 1999, Long-distance transport of magmas in the
879 Jurassic Ferrar Large Igneous Province, Antarctica: Earth and Planetary Science Letters, v. 167, p.
880 89-104.
881 Faure, G., and Mensing, T. M., 2010, The Transantarctic Mountains: Rocks, ice, meteorites and water,
882 Springer Science & Business Media.
883 Fitzpatrick, J. J., Muhs, D. R., and Jull, A. J. T., 1990, Saline minerals in the Lewis Cliff Ice Tongue,
884 Antarctic Research Series, Volume Contributions to Antarctic Research I, p. 57-69.
885 Gaillardet, J., Dupré, B., Louvat, P., and Allègre, C. J., 1999, Global silicate weathering and CO_2
886 comsumption rates deduced from the chemistry of large rivers: Chemical Geology, v. 159, p. 3-
887 30.
888 Golledge, N. R., Levy, R. H., McKay, R. M., Fogwill, C. J., White, D. A., Graham, A. G. C., Smith, J. A.,
889 Hillenbrand, C.-D., Licht, K. J., Denton, G. H., Ackert, R. P., Maas, S. M., and Hall, B. L., 2013,
890 Glaciology and geological signature of the Last Glacial Maximum Antarctic ice sheet: Quaternary
891 Science Reviews, v. 78, p. 225-247.
892 Gooch, B. T., Young, D. A., and Blankenship, D. D., 2016, Potential groundwater and heterogeneous heat
893 source contributions to ice sheet dynamics in critical submarine basins of East Antarctica:
894 Geochemistry, Geophysics, Geosystems, v. 17, no. 2, p. 395-409.
895 Goodwin, I., 1988, The nature and origin of a jökulhlaup near Casey Station, Antarctica: Journal of
896 Glaciology, v. 34, no. 116, p. 95-101.
897 Gow, A. J., and Williamson, T., 1975, Gas inclusions in the Antarctic ice sheet and their glaciological
898 significance: Journal of Geophysical Research, v. 80, no. 36, p. 5101-5108.
899 Graly, J. A., Drever, J. I., and Humphrey, N. F., 2017, Calculating the balance between atmospheric CO_2
900 drawdown and organic carbon oxidation in subglacial hydrochemical systems: Global
901 Biogeochemical Cycles, v. 31, no. 4, p. 709-727.
902 Graly, J. A., Humphrey, N. F., and Harper, J. T., 2016, Chemical depletion of sediment under the
903 Greenland Ice Sheet: Earth Surface Processes and Landforms, v. 41, no. 13, p. 1922-1936.
904 Graly, J. A., Humphrey, N. F., Landowski, C. M., and Harper, J. T., 2014, Chemical weathering under the
905 Greenland Ice Sheet: Geology, v. 42, p. 551-554.
906 Graly, J. A., Humphrey, N. F., and Licht, K. J., 2018a, Two Metrics Describing the Causes of Seasonal and
907 Spatial Changes in Subglacial Aqueous Chemistry: Frontiers in Earth Science, v. 6, no. 195.
908 Graly, J. A., Licht, K. J., Drushel, G. K., and Kaplan, M. R., 2018b, Polar desert chronologies through
909 quantitative measurements of salt accumulation: Geology, v. 46, p. 351-354.
910 Graly, J. A., Licht, K. J., Kassab, C. M., Bird, B. W., and Kaplan, M. R., 2018c, Warm-based basal sediment
911 entrainment and far-field Pleistocene origin evidenced in central Transantarctic blue ice through
912 stable isotopes and internal structures: Journal of Glaciology, v. 64, p. 185-196.
913 Haldorsen, S., 1981, Grain-size distribution of subglacial till and its realtion to glacial scrushing and
914 abrasion: Boreas, v. 10, no. 1, p. 91-105.
915 Hawkings, J. R., Wadham, J. L., Benning, L. G., Hendry, K. R., Tranter, M., Tedstone, A., Nienow, P., and
916 Raiswell, R., 2017, Ice sheets as a missing source of silica to the polar oceans: Nature
917 communications, v. 8, p. 14198.
918 Hodson, A., Tranter, M., and Vatne, G., 2000, Contemporary rate of chemical denudation and
919 atmospheric CO_2 sequestration in glacier basins: An arctic perspective: Earth Surface Processes
920 and Landforms, v. 25, p. 1447-1471.
921 Horner, T. C., 1992, Sedimentological, mineralogical, and geochemical evaluation of the provenance and
922 paleoclimatic record of Permian mudrocks from the Beardmore Glacier area, Antarctica [Ph.D.:
923 The Ohio State University.

924 Isbell, J. L., 1990, Fluvial sedimentology and basin analyses of the Permian Fairchild and Buckley
925 Formations, Beardmore Glacier region, and the Weller Coal Measures, Southern Victoria Land,
926 Antarctica: The Ohio State University.
927 Iverson, N. R., and Semmens, D. J., 1995, Intrusion of ice porous media by regelation: A mechanism of
928 sediment entrainment by glaciers: Journal of Geophysical Research, v. 100, no. B7, p. 10219-
929 10230.
930 Jamieson, S. S. R., Sugden, D. E., and Hulton, R. J., 2010, The evolution of the subglacial landscape of
931 Antarctica: Earth and Planetary Science Letters, v. 293, p. 1-27.
932 Kaplan, M. R., Licht, K. J., Winckler, G., Schaefer, J. M., Bader, N., Mathieson, C., Roberts, M., Kassab, C.
933 M., Schwartz, R., and Graly, J. A., 2017, Mid-Late Pleistocene stability of the central East
934 Antarctic Ice Sheet at the head of Law Glacier: Geology, v. 45, no. 11, p. 963-966.
935 Kassab, C. M., Licht, K. J., Petersson, R., Lindbäck, K., Graly, J. A., and Kaplan, M. R., 2020, Formation and
936 evolution of an extensive blue ice moraine in central Transantarctic Mountains, Antarctica:
937 Journal of Glaciology, v. 66, p. 49-60.
938 Kump, L. R., Brantley, S. L., and Arthur, M. A., 2000, Chemical weathering, atmospheric CO_2 and climate:
939 Annual Review of Earth and Planetary Sciences, v. 28, p. 611-667.
940 La Prade, K. E., 1972, Petrology and petrography of the Beacon Supergroup, Shackleton Glacier area,
941 Queen Maud Range, Transantarctic Mountains, Antarctica, Proceedings of the third symposium
942 on Antarctic geology and geophysics: Madison, Wisconsin, USA, The University of Wisconsin
943 Press, p. 581-590.
944 Lee, A., and Rutter, E., 2004, Experimental rock-on-rock frictional wear: Application to subglacial
945 abrasion: Journal of Geophysical Research: Solid Earth, v. 109, no. B9.
946 Legrand, M., and Mayewski, P., 1997, Glaciochemistry of polar ice cores: A review: Reviews of
947 Geophysics, v. 35, no. 3, p. 219-243.
948 Liu, T., Bish, D. L., Socki, R. A., Harvey, R. P., and Tonui, E., 2014, Mineralogy and formation of evaporite
949 deposits from the Lewis Cliff ice tongue, Antarctica: Antarctic Science, v. 27, no. 1, p. 73-84.
950 Michaud, A. B., Skidmore, M. L., Mitchell, A. C., Vick-Majors, T. J., Barbante, C., Turetta, C., vanGelder,
951 W., and Priscu, J. C., 2016, Solute sources and geochemical processes in Subglacial Lake
952 Whillans, West Antarctica: Geology, v. 44, no. 5, p. 347-350.
953 Mikucki, J. A., Foreman, C. M., Sattler, B., Lyons, W. B., and Priscu, J. C., 2004, Geomicrobiology of Blood
954 Falls: an iron-rich saline discharge at the terminus of the Taylor Glacier, Antarctica: Aquatic
955 Geochemistry, v. 10, no. 3-4, p. 199-220.
956 Moulton, K. L., West, J., and Berner, R. A., 2000, Solute flux and mineral mass balance approaches to the
957 quantification of plant effects on silicate weathering: American Journal of Science, v. 300, no. 7,
958 p. 539-570.
959 Pattyn, F., 2010, Antarctic subglacial conditions inferred from a hybrid ice sheet/ice stream model: Earth
960 and Planetary Science Letters, v. 295, p. 451-461.
961 Petsch, S. T., 2014, Weathering of organic carbon: Treatise on Geochemistry (Elsevier, ed. 2), v. 12, p.
962 217-238.
963 Pollard, D., and DeConto, R. M., 2009, Modelling West Antarctic ice sheet growth and collapse through
964 the past five million years: Nature, v. 458, no. 7236, p. 329.
965 Rempel, A. W., 2008, A theory for ice-till interactions and sediment entrainment beneath glaciers:
966 Journal of Geophysical Research, v. 113, p. F01013.
967 Reynolds, R., 1989, Diffraction by small and disordered crystals, *in* Bish, D. L., and Post, J. E., eds.,
968 Modern Powder Difraction, Volume 20, p. 145-182.
969 Rietveld, H. M., 1969, A profile refinement method for nuclear and magnetic structures: Journal of
970 applied Crystallography, v. 2, no. 2, p. 65-71.

971 Rignot, E., Mouginot, J., and Scheuchl, B., 2011, Ice flow of the Antarctic Ice Sheet: Science, v. 333, p.
972 1427-1430.
973 Scarrow, J. W., Balks, M. R., and Almond, P. C., 2014, Three soil chronosequences in recessional glacial
974 deposits near the polar plateau, in the Central Transantarctic Mountains, Antarctica: Antarctic
975 Science, v. 26, no. 5, p. 573-583.
976 Scherer, R. P., DeConto, R. M., Pollard, D., and Alley, R. B., 2016, Windblown Pliocene diatoms and East
977 antarctic ice sheet retreat: Nature communications, v. 7, p. 12957.
978 Setti, M., Marinoni, L., and Lopez-Galindo, A., 2004, Mineralogical and geochemical characteristics
979 (major, minor, trace elements and REE) of detrital and authigenic clay minerals in a Cenozoic
980 sequence from Ross Sea, Antarctica, De Gruyter.
981 Sharp, M., and Gomez, B., 1986, Processes of debris comminution in the glacial environment and
982 implications for quartz sand-grain morphology: Sedimentary Geology, v. 46, p. 33-47.
983 Siegert, M. J., Kulessa, B., Bougamont, M., Christoffersen, P., Key, K., Andersen, K. R., Booth, A. D., and
984 Smith, A. M., 2018, Antarctic subglacial groundwater: a concept paper on its measurement and
985 potential influence on ice flow: Geological Society, London, Special Publications, v. 461, no. 1, p.
986 197-213.
987 Skidmore, M., Tranter, M., Tulaczyk, S., and Lanoil, B., 2010, Hydrochemistry of ice stream beds -
988 evaporitic or microbial effects?: Hydrological Processes, v. 24, p. 517-523.
989 Smith, B. E., Fricker, H. A., Joughin, I. R., and Tulaczyk, S., 2009, An inventory of active subglacial lakes in
990 Antarctica detected by ICESat (2003–2008): Journal of Glaciology, v. 55, no. 192, p. 573-595.
991 Sun, T., Socki, R. A., Bish, D. L., Harvey, R. P., Bao, H., Niles, P. B., Cavicchioli, R., and Tonui, E., 2015, Lost
992 cold Antarctic deserts inferred from unusual sulfate formation and isotope signatures: Nature
993 Communications.
994 Tessier, A., Campbell, P. G. C., and Bisson, M., 1979, Sequential extraction prodecudre for the speciation
995 of particulate trace metals: Analytical Chemistry, v. 51, no. 7, p. 844-851.
996 Torres, M. A., Moosdorf, N., Hartmann, J., Adkins, J. F., and West, A. J., 2017, Glacial weathering, sulfide
997 oxidation, and global carbon cycle feedbacks: Proceedings of the National Academy of Sciences,
998 v. 114, no. 33, p. 8716-8721.
999 Tranter, M., 2003, Geochemical weathering in glacial and proglacial environments: Treatise on
1000 geochemistry, v. 5, p. 189-205.
1001 Tranter, M., Sharp, M. J., Lamb, H. R., Brown, G. H., Hubbard, B. P., and Willis, I. C., 2002, Geochemical
1002 weathering at the bed of the Haut Glacier d'Arolla, Switzerland - a new model: Hydrological
1003 Processes, v. 16, p. 959-993.
1004 Tulaczyk, S. M., 1999, Basal mechanics and geologic record of ice streaming, West Antarctica: California
1005 Institute of Technology.
1006 Vavra, C. L., 1989, Mineral reactions and controls on zeolite facies alteration in sandstone of the Central
1007 Transantarctic Mountains, Antarctica: Journal of Sedimentary Petrology, v. 59, no. 5, p. 688-703.
1008 Vennum, W. R., and Nejedly, J. W., 1990, Clay mineralogy of soils developed on weathered igneous
1009 rocks, West Antarctica: New Zealand Journal of Geology and Geophysics, v. 33, no. 4, p. 579-
1010 584.
1011 Wadham, J. L., Arndt, S., Tulaczyk, S., Stibal, M., Tranter, M., Telling, J., Lis, G. P., Lawson, E., Ridgwell, A.,
1012 Dubnick, A., Sharp, M. J., Anesio, A. M., and Butler, C. E. H., 2012, Potential methane reservoirs
1013 beneath Antarctica: Nature, v. 488, p. 633-637.
1014 Wadham, J. L., Tranter, M., Skidmore, M., Hodson, A. J., Priscu, J., Lyons, W. B., Sharp, M., Wynn, P., and
1015 Jackson, M., 2010, Biogeochemical weathering under ice: Size matters: Global Biogeochemical
1016 Cycles, v. 24, p. GB3025.

1017 Wand, U., Schwarz, G., Brüggemann, E., and Bräuer, K., 1997, Evidence for physical and chemical
1018 stratification in Lake Untersee (central Dronning Maud Land, East Antarctica): Antarctic Science,
1019 v. 9, no. 1, p. 43-45.
1020 Wiederhold, J. G., Teutsch, N., Kraemer, S. M., Halliday, A. N., and Kretzschmar, R., 2007, Iron isotope
1021 fractionation in oxic soils by mineral weathering and podzolization: Geochimica et
1022 Cosmochimica Acta, v. 71, p. 5821-5833.
1023 Wilson, D. S., Jamieson, S. S. R., Barrett, P. J., Leitchenkov, G., Gohl, K., and Larter, R. D., 2012, Antarctic
1024 topography at the Eocene–Oligocene boundary: Palaeogeography, Palaeoclimatology,
1025 Palaeoecology, v. 335-336, p. 24-34.
1026 Wilson, M. J., 1999, The origin and formation of clay minerals in soils: past, present and future
1027 perspectives: Clay Minerals, v. 34, p. 7-25.
1028 Wingham, D. J., Siegert, M. J., Shepherd, A., and Muir, A. S., 2006, Rapid discharge connects Antarctic
1029 subglacial lakes: Nature, v. 440, no. 7087, p. 1033.
1030 Wright, A., and Siegert, M., 2012, A fourth inventory of Antarctic subglacial lakes: Antarctic Science, v.
1031 24, no. 6, p. 659-664.

1032

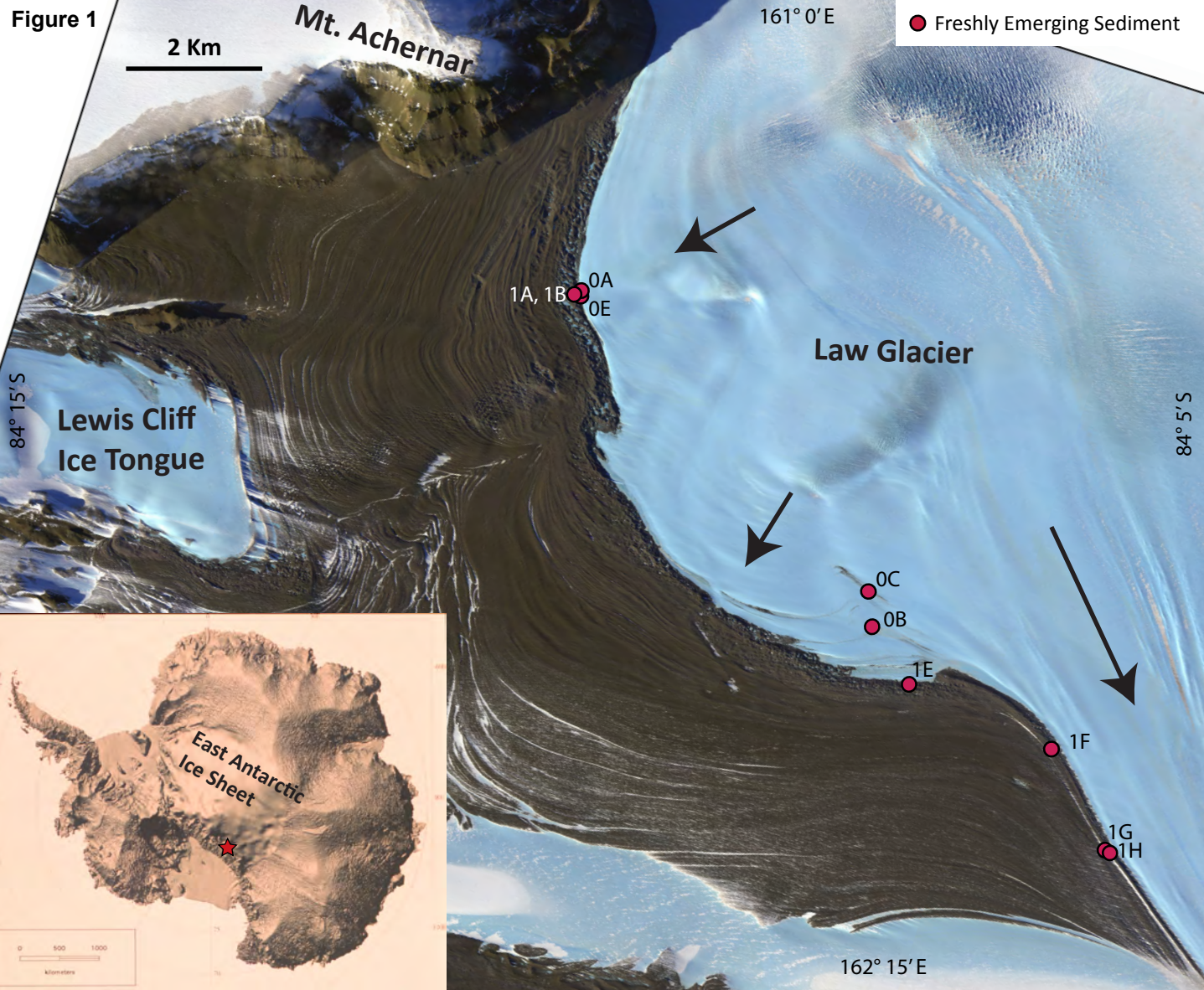
Figure 1
2 Km
Mt. Achernar
161° 0′ E
Freshly Emerging Sediment
1A, 1B
0A
0E
Law Glacier
84° 15′ S
Lewis Cliff
Ice Tongue
84° 5′ S
0C
0B
1E
1F
1G
1H
162° 15′ E
East Antarctic
Ice Sheet

Figure 2

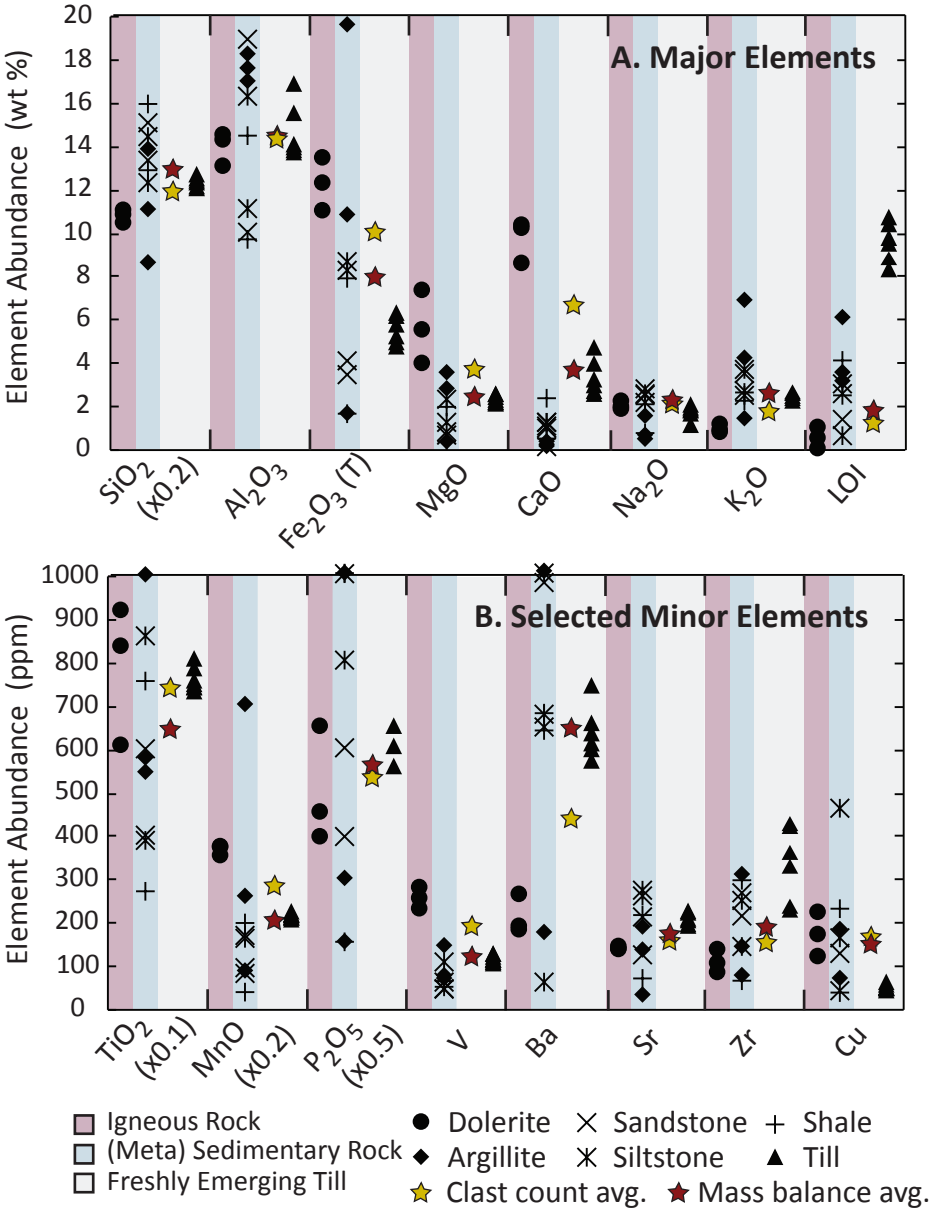
A. Major Elements
Element Abundance (wt %)
20
18
16
14
12
10
8
6
4
2
0
SiO2 (x0.2)
Al2O3
Fe2O3 (T)
MgO
CaO
Na2O
K2O
LOI
B. Selected Minor Elements
Element Abundance (ppm)
1000
900
800
700
600
500
400
300
200
100
0
TiO2 (x0.1)
MnO (x0.2)
P2O5 (x0.5)
V
Ba
Sr
Zr
Cu
Igneous Rock
(Meta) Sedimentary Rock
Freshly Emerging Till
Dolerite
Argillite
Sandstone
Siltstone
Shale
Till
Clast count avg.
Mass balance avg.

Figure 2 Cont.

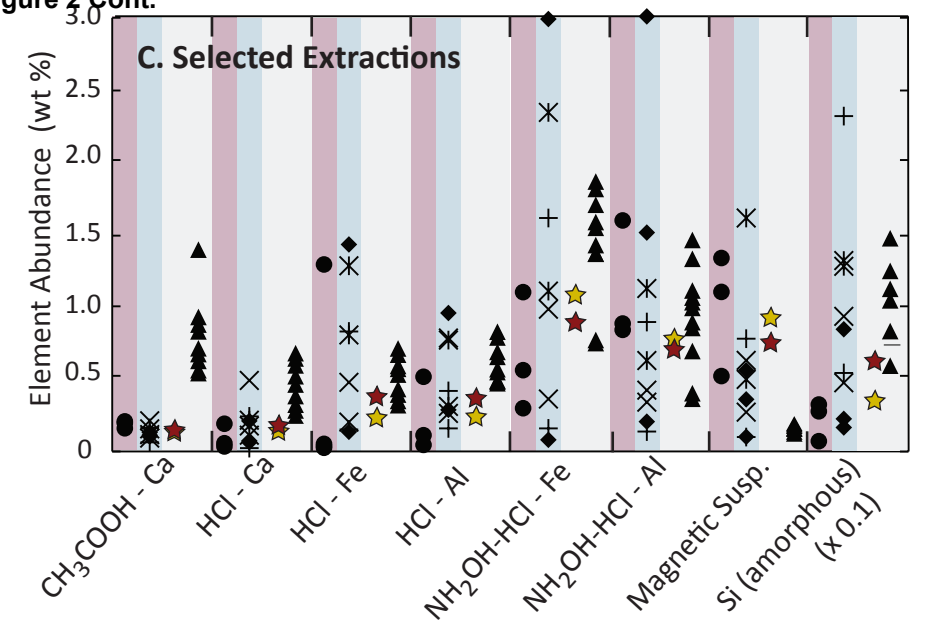

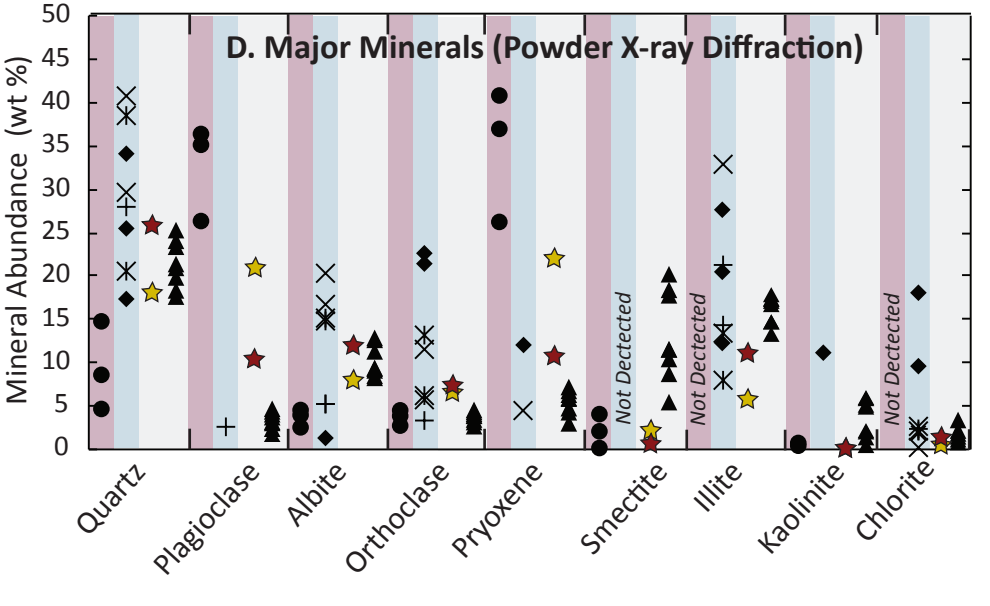

Figure 3

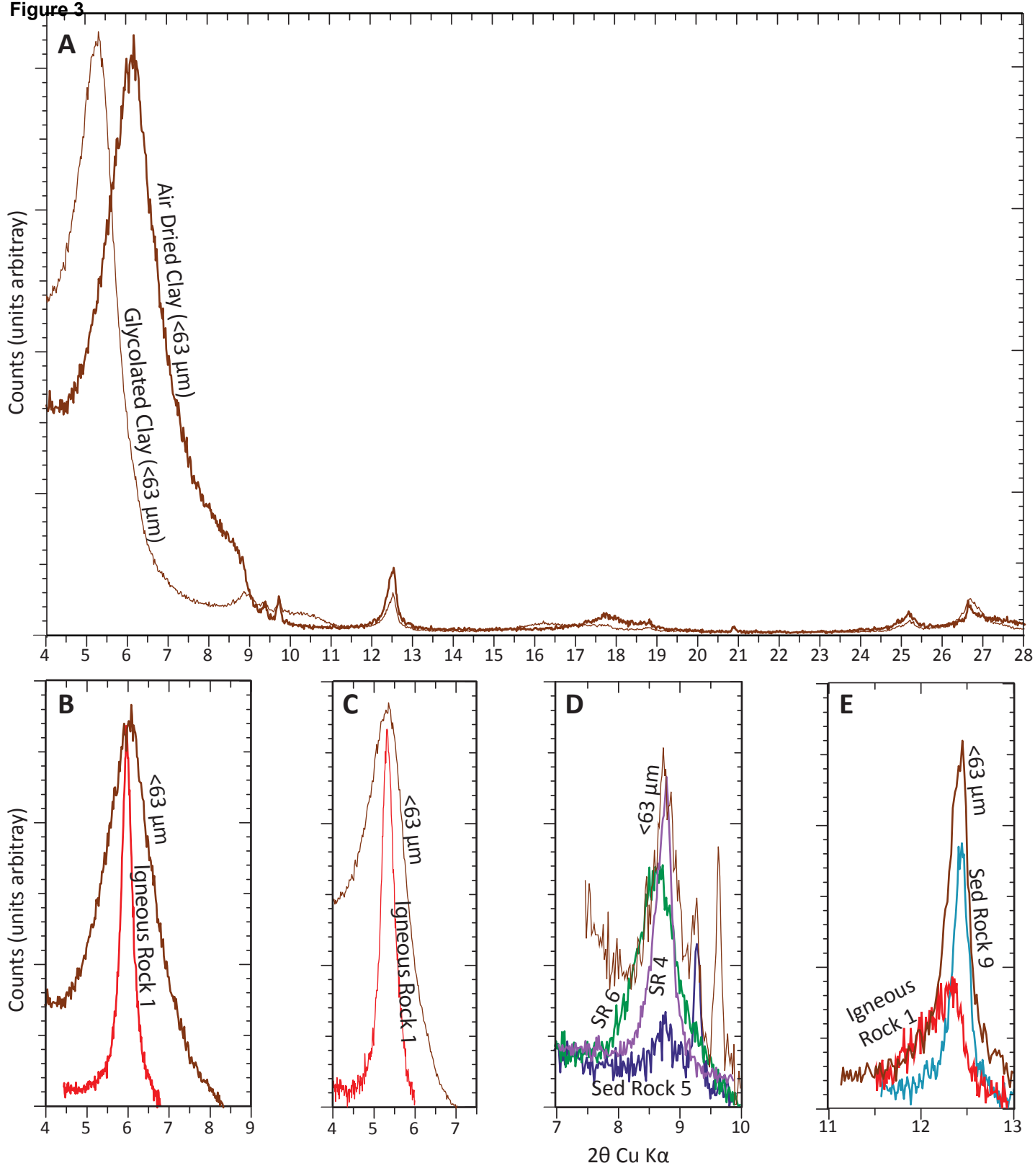
A
Air Dried Clay (<63 µm)
Glycolated Clay (<63 µm)
Counts (units arbitray)
4 5 6 7 8 9 10 11 12 13 14 15 16 17 18 19 20 21 22 23 24 25 26 27 28
B
<63 µm
Igneous Rock 1
C
<63 µm
Igneous Rock 1
D
<63 µm
SR 6
SR 4
Sed Rock 5
E
<63 µm
Sed Rock 9
Igneous Rock 1
4 5 6 7 8 9
4 5 6 7
7 8 9 10
11 12 13
2θ Cu Kα

Figure 4

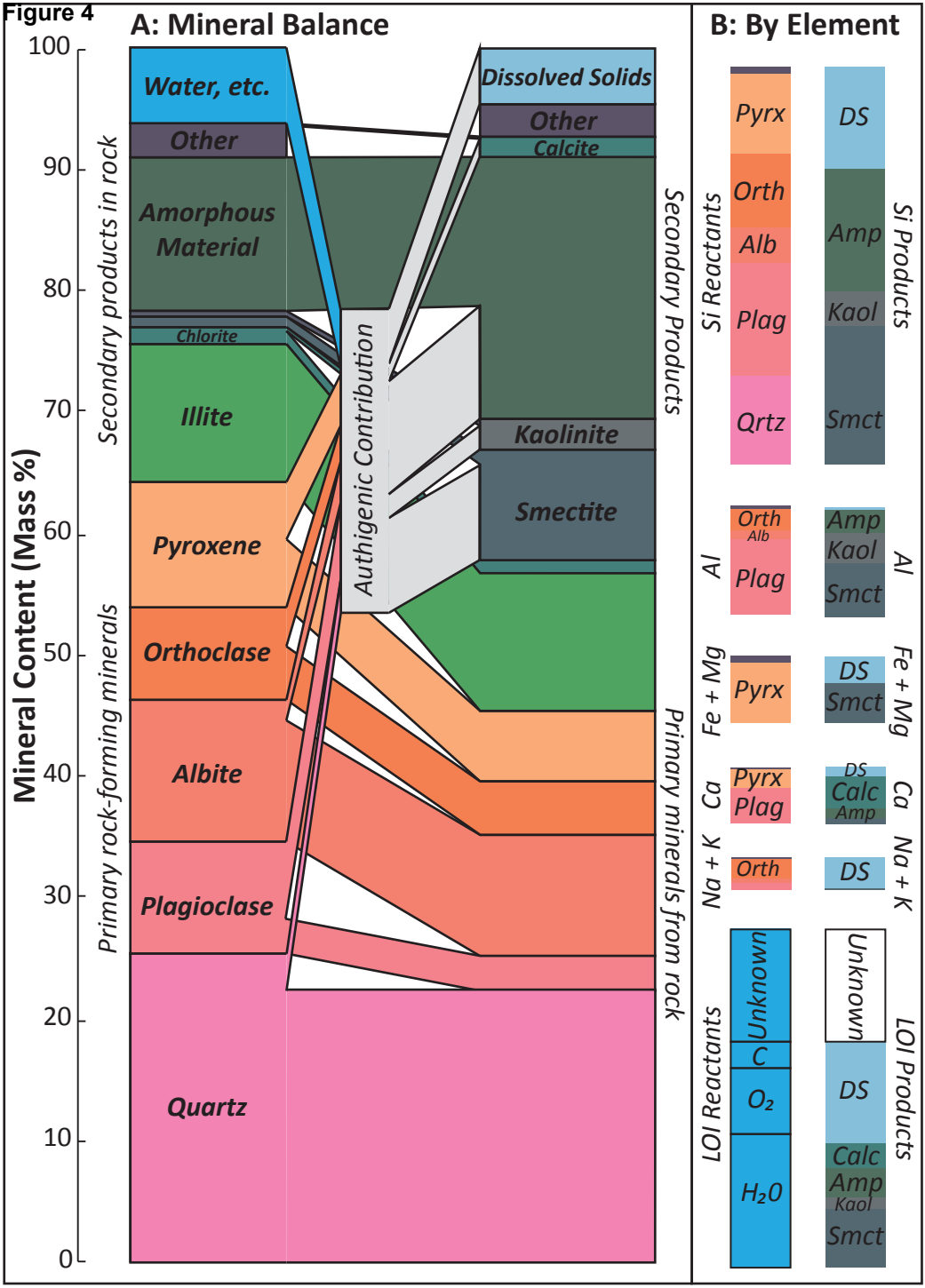
A: Mineral Balance
B: By Element
Mineral Content (Mass %)
100
90
80
70
60
50
40
30
20
10
0
Secondary products in rock
Primary rock-forming minerals
Water, etc.
Other
Amorphous Material
Chlorite
Illite
Pyroxene
Orthoclase
Albite
Plagioclase
Quartz
Authigenic Contribution
Dissolved Solids
Other
Calcite
Kaolinite
Smectite
Secondary Products
Primary minerals from rock
Si Reactants
Pyrx
Orth
Alb
Plag
Qrtz
Si Products
DS
Amp
Kaol
Smct
Al
Orth
Alb
Plag
Amp
Kaol
Smct
Fe + Mg
Pyrx
DS
Smct
Ca
Pyrx
Plag
DS
Calc
Amp
Na + K
Orth
DS
LOI Reactants
Unknown
C
O₂
H₂0
LOI Products
Unknown
DS
Calc
Amp
Kaol
Smct

Figure 5

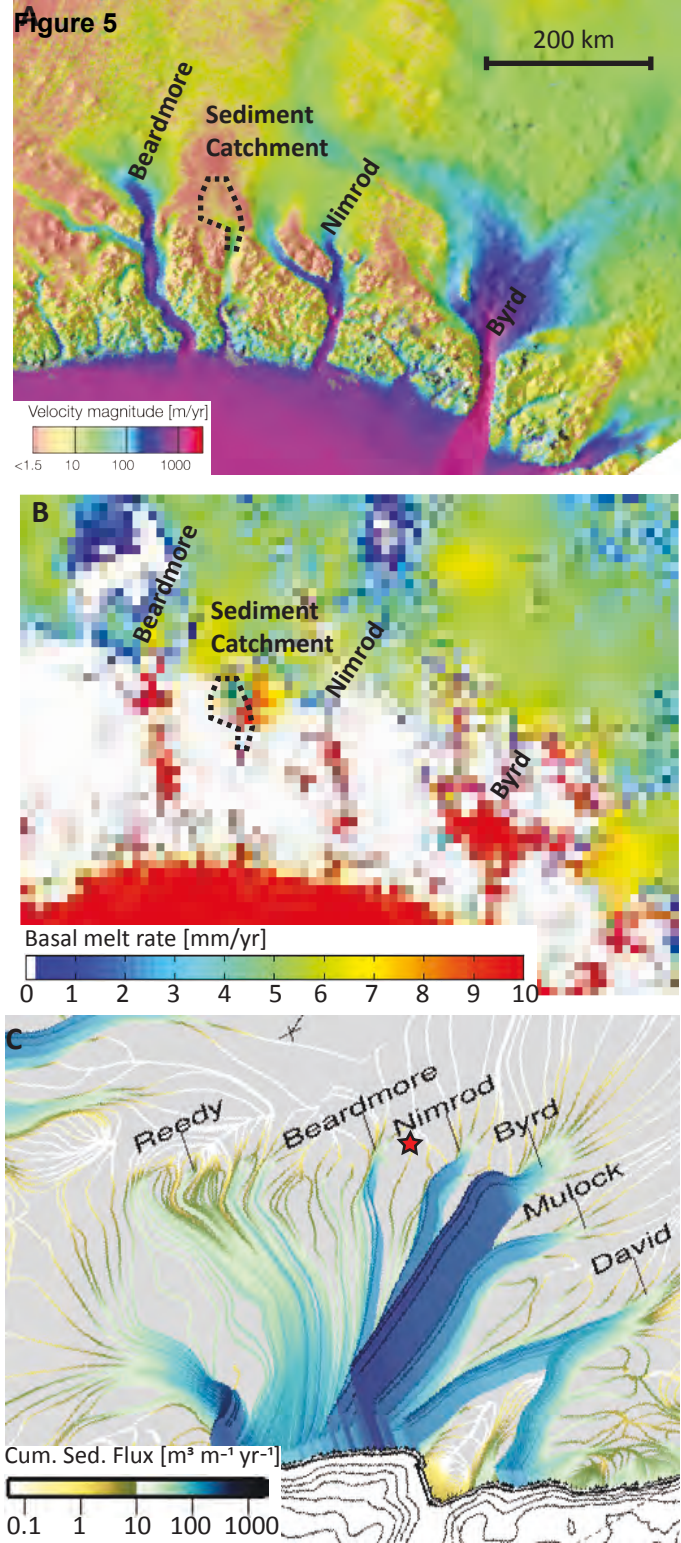
A
200 km
Beardmore
Sediment
Catchment
Nimrod
Byrd
Velocity magnitude [m/yr]
<1.5
10
100
1000
B
Beardmore
Sediment
Catchment
Nimrod
Byrd
Basal melt rate [mm/yr]
0
1
2
3
4
5
6
7
8
9
10
C
Reedy
Beardmore
Nimrod
Byrd
Mulock
David
Cum. Sed. Flux [m³ m⁻¹ yr⁻¹]
0.1
1
10
100
1000

Figure 6

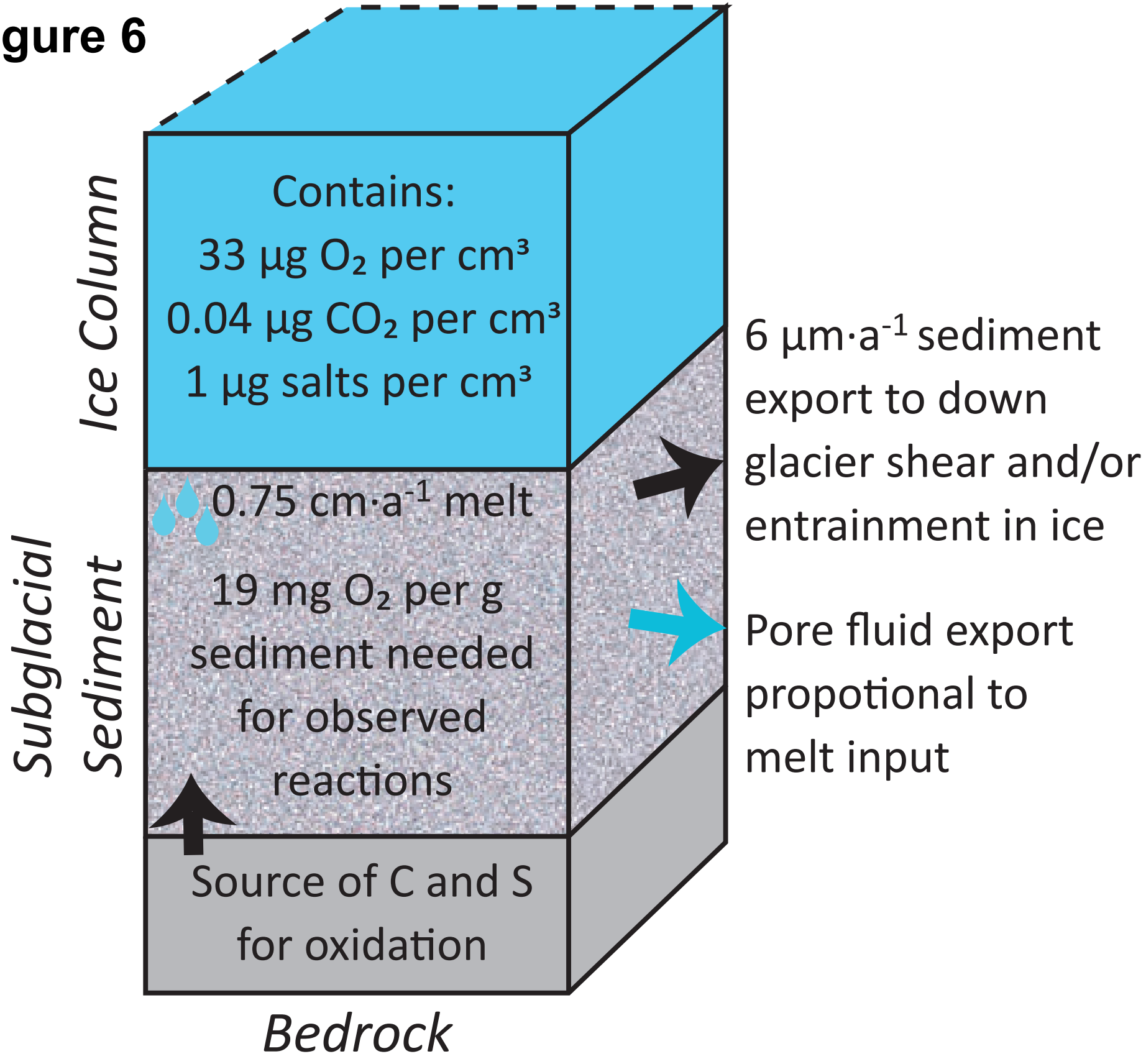
Ice Column
Contains:
33 µg O_2 per cm³
0.04 µg CO_2 per cm³
1 µg salts per cm³
Subglacial Sediment
0.75 cm·a^{-1} melt
19 mg O_2 per g sediment needed for observed reactions
Source of C and S for oxidation
Bedrock
6 µm·a^{-1} sediment export to down glacier shear and/or entrainment in ice
Pore fluid export propotional to melt input

Figure 7

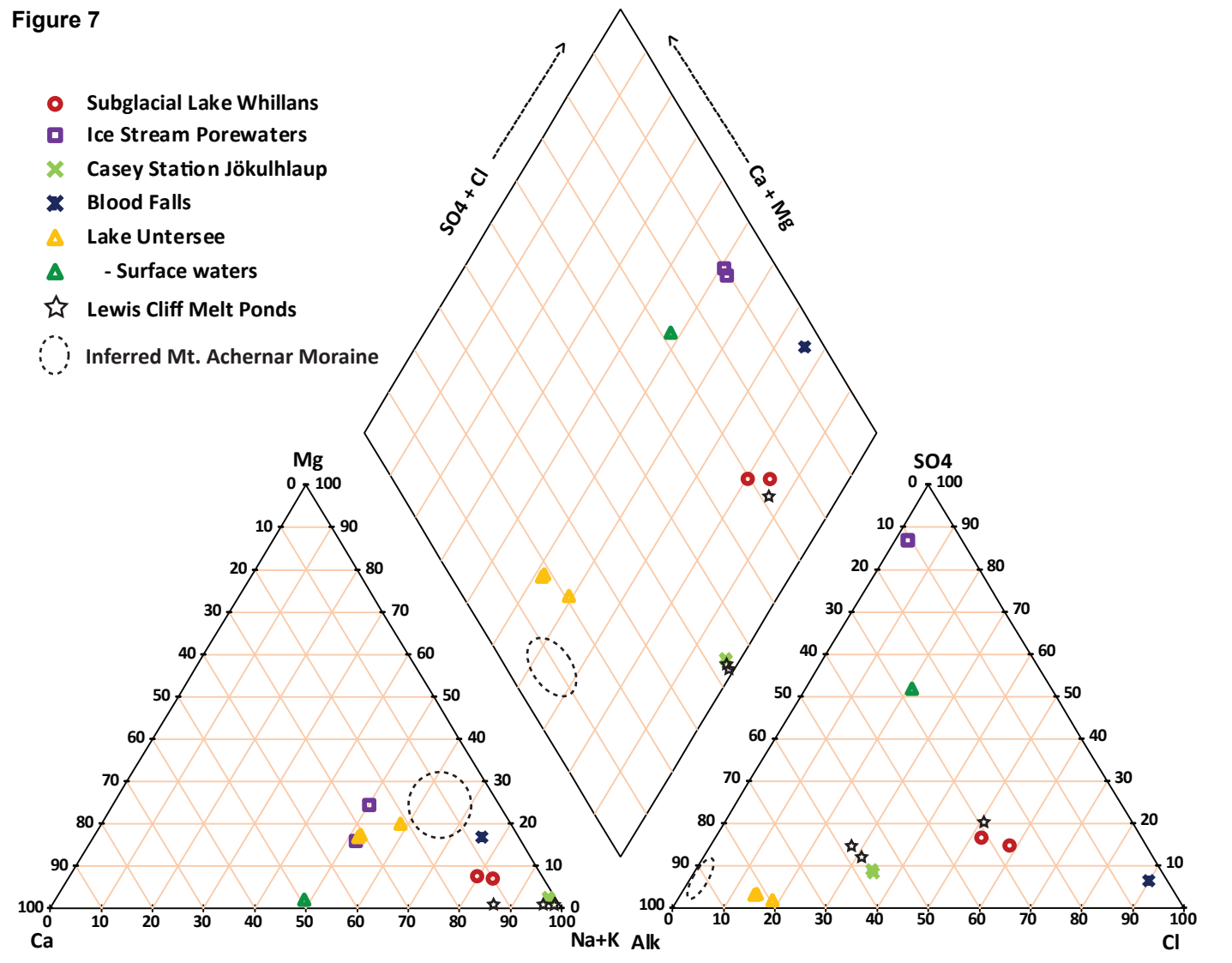
Subglacial Lake Whillans
Ice Stream Porewaters
Casey Station Jökulhlaup
Blood Falls
Lake Untersee
- Surface waters
Lewis Cliff Melt Ponds
Inferred Mt. Achernar Moraine
SO4 + Cl
Ca + Mg
Mg
Ca
Na+K
SO4
Alk
Cl

Figure 8

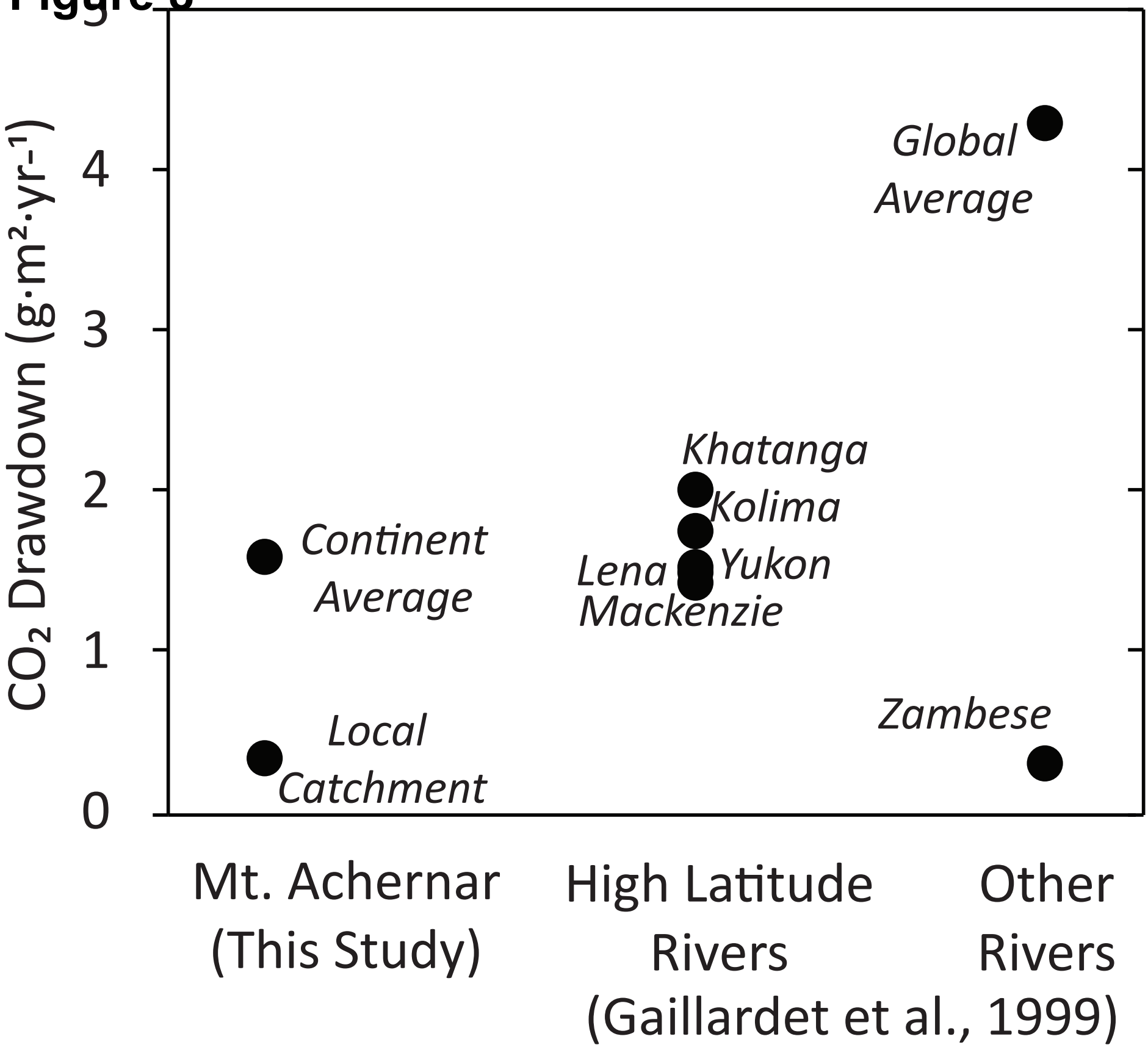
CO_2 Drawdown ($g \cdot m^2 \cdot yr^{-1}$)
0
1
2
3
4
Global Average
Khatanga
Kolima
Yukon
Lena
Mackenzie
Continent Average
Local Catchment
Zambese
Mt. Achernar (This Study)
High Latitude Rivers (Gaillardet et al., 1999)
Other Rivers

Electronic Annex

Click here to download Electronic Annex: Gralyetal_Supplemental.xlsx

***Declaration of Interest Statement**

Declaration of interests

☒ The authors declare that they have no known competing financial interests or personal relationships that could have appeared to influence the work reported in this paper.

☐The authors declare the following financial interests/personal relationships which may be considered as potential competing interests: